# Continuum theory of memory effect in crack patterns of drying pastes

Ooshida Takeshi（大信田丈志）*

*Department of Applied Mathematics and Physics, Tottori University, JP-680-8552, Japan*
(Received 14 September 2007; published 3 June 2008)

A possible clarification of memory effect observed in crack patterns of drying pastes [A. Nakahara and Y. Matsuo, J. Phys. Soc. Jpn. **74**, 1362 (2005)] is presented in terms of a macroscopic elastoplastic model of isotropic pastes. We study flows driven by steady gravitational force instead of external oscillation. The model predicts creation of residual tension in favor of cracks perpendicular to the flow direction, thus causing the same type of memory effect as that reported by Nakahara and Matsuo for oscillated $CaCO_3$ pastes.

## I. INTRODUCTION

As the plastic behavior of soft glassy materials has been attracting increasing interest [1], it was reported by Nakahara and Matsuo [2–4] that a drying paste exhibits a memory effect. They observed a drying process for a paste containing calcium carbonate ($CaCO_3$) and water in a shallow container in order to study the resulting crack pattern. The crack pattern was typically found to be isotropic, but they discovered a way to introduce anisotropy into the paste *before* the drying process commences: by applying a horizontal oscillation to the container immediately after the paste is poured into it, a memory of the oscillation is imprinted into the paste, which determines how it should break in the future.

Through systematic experiments, Nakahara and Matsuo also found that plasticity is essential to the memory effect in $CaCO_3$ pastes. No memory effect is observed if the strength of the applied oscillation is below the threshold value corresponding to the plastic yield stress of the paste. Just above the threshold value, the paste remembers the oscillation that caused the plastic flow, developing cracks perpendicular to the direction of the oscillation. If the oscillation is too strong or the paste contains too much water, waves and global flows are induced, eliminating the memory effect. A different kind of paste (mixture of magnesium carbonate hydroxide with water) [5] exhibits not only a memory effect similar to that of $CaCO_3$ that occurs just above the threshold of plastic flows and causes cracks perpendicular to the external oscillation, but also a different type of memory effect in its water-rich condition where the cracks are parallel to the direction of the global laminar flow caused by the oscillation. Too strong an oscillation and too much water also destroy the memory in this paste, with the emergence of chaotic, turbulencelike flows [49] characterized by fluid motion in every direction.

Here we focus our attention on the former type of memory effect that causes cracks perpendicular to the external forcing, which we refer to as the type-I Nakahara effect. The latter type, which could be called the type-II Nakahara effect, will be discussed only briefly.

Although it is certain that the memory effect in $CaCO_3$ pastes originates from plastic flow, it is unclear which as-

pects of the plastic flow are essential. More specifically, because the role played by the unsteadiness of the flow is not fully understood, it is unknown whether a slope flow, in which the external forcing is steady, can cause a memory effect. To answer this question, co-workers of the present author have started an experimental study on the slope flow of $CaCO_3$ paste. Paste supplied through a funnel is driven downstream by gravitational force, and when the supply is stopped, the paste "freezes" at some finite thickness due to the finite yield stress. Preliminary results suggest the presence of a memory effect (type-I Nakahara effect), where the cracks are perpendicular to the direction of the flow, i.e., the direction of the external forcing. Details of the experiment will be reported elsewhere [6].

As a first step in the theoretical investigation into the slope flow of $CaCO_3$ paste, we study the dynamics of an elastoplastic liquid layer with constant thickness falling down an inclined wall. First, we construct a continuum model equation that meets several requirements, so that it can be a good description of the $CaCO_3$ paste. Next, we apply this model equation to the two-dimensional slope flow with constant layer thickness. We find that the flow develops *tension* in the streamwise direction, which remains in the paste. Since the residual tension implies that the dried paste will be more fragile in the pertinent direction, this result presents a possible clarification of the type-I Nakahara effect.

## II. REQUIREMENTS FOR THE MODEL

The strategy in this paper includes the construction of a set of model equations acceptable as a continuum description of $CaCO_3$ paste. A useful precedent for this model construction can be found in the continuum mechanics of gases and simple liquids [7,8], in which the Navier-Stokes equation is deduced from several macroscopic requirements, such as homogeneity, isotropy, and the postulation that the deviatoric stress tensor is a linear function of the rate-of-strain tensor (without time lag). Following this precedent, let us list the analogous requirements for paste flows.

We assume that the dynamics of the paste is isotropic, in the sense that the paste has no preferred direction except for the principal axes of the stress tensor. This is plausible for $CaCO_3$, which consists of spherical particles [3,4]. On the other hand, magnesium carbonate hydroxide is not expected to exhibit isotropy in this sense, as its particles are disklike

─────────
*ooshida@damp.tottori-u.ac.jp

[5] and therefore can exhibit anisotropy similar to that of liquid crystals.

The stresses in the pastes under present consideration are primarily sustained by the interparticulate bond network. There should be also a contribution from the viscosity of the solvent (water), but we assume that this contribution is much smaller than that of the interparticulate bonds (in other words, we consider only very thick colloids). Unlike the chemical bonds, the interparticulate bonds in flowing pastes are usually so breakable that they are constantly destroyed and reconstructed. The stress is therefore expected to be governed by a Maxwell-type equation [9–13]. whose relaxation time represents the lifetime of the bond.

We postulate that the relaxation time, denoted by $\tau$, is a scalar: the collapse of the force network involves bond breakage in all directions. Since the paste is plastic, the relaxation time $\tau$ must be variable. An infinitely large $\tau$ represents solidlike behavior, while a finite $\tau$ denotes fluidity. The transition between these two behaviors with a certain threshold gives a formulation of plasticity. Isotropy dictates not only that $\tau$ itself is a scalar, but also that $\tau$ should be a function of some scalar quantity. With the von Mises criterion [14] and its energetic interpretation [15] in mind, we assume that the relaxation time $\tau$ is a function of strain energy. Introducing $\varepsilon$ to denote the nondimensionalized strain energy (defined later), this assumption is formulated as

$$\tau = \tau(\varepsilon) \sim \begin{cases} +\infty & (\varepsilon < \text{threshold}) \\ \tau_0 = \eta_{\mathrm{p}}/S & (\varepsilon \gg \text{threshold}), \end{cases} \quad (1)$$

where $\eta_{\mathrm{p}}$ is a constant with the dimension of viscosity, and $S$ is the shear modulus.

We describe the relaxation of the bond network in terms of the Lagrangian (material) variable $\boldsymbol{\xi}$, rather than the Eulerian variable $\mathbf{r}$. The main reason for this choice is the adequacy of the Lagrangian description for tracing so-called frozen quantities. With the relevant physical quantity provisionally symbolized as $\mathcal{G}$ (probably representative of the density of the bond network), the equation of relaxation is expected to have the form

$$\left(1 + \tau \frac{\partial}{\partial t}\right) \mathcal{G}(\boldsymbol{\xi}, t) = \mathcal{G}_*(\boldsymbol{\xi}, t). \quad (2)$$

In the limit of an infinitely long relaxation time ($\tau \to +\infty$), Eq. (2) reduces itself to

$$\partial_t \mathcal{G}(\boldsymbol{\xi}, t) = 0 \quad (3)$$

which manifests directly that $\mathcal{G}$ is "frozen" in the material. In the Eulerian description, the same assertion as Eq. (3) would have a more complicated form,

$$(\partial_t + \mathbf{v} \cdot \nabla)\widetilde{\mathcal{G}}(\mathbf{r}, t) + \cdots = 0 \quad \text{(Eulerian)}, \quad (4)$$

where "⋯" stands for various convective terms required according to the tensorial character of $\widetilde{\mathcal{G}}$. Since we prefer the clarity of Eq. (3) to the obscurity of Eq. (4), the Lagrangian description is adopted during the construction of the model (the result could be reformulated in the Eulerian description *after* it is developed, of course).
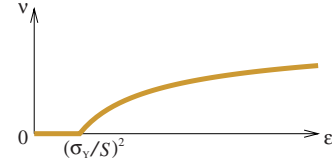


FIG. 1. (Color online) The inverse of the relaxation time, $\tau^{-1} = \nu(\varepsilon)$, defined by Eq. (29). According to neo-Hookian constitutive equation of $n_d$-dimensional elastic bodies, $\varepsilon$ is given by Eq. (23).

Generally, the mathematical formulation of elasticity is related to the *deformation* of the fluid (or material) elements. In the steady and quasisteady motions of pastes, deformation (as opposed to *rate of deformation*) can increase unlimitedly as the time elapses. This requires our model to be free from the restrictive assumption of a small deformation, motivating the inclusion of the geometrical nonlinearity to the full extent. Besides, the solid behavior of the paste for a small deformation should have an isotropic Hookian limit (with shear modulus $S$), because the paste is isotropic. For the same reason, the fluid behavior is expected to have a Navier-Stokes limit for small $\tau$ or small shear rate (which is realized for water-rich pastes with a vanishingly small yield stress). In both behaviors, we regard the paste as incompressible, as far as flow processes are concerned, neglecting the slow effects of drainage and evaporation. Finally, the model equation must have "relabeling symmetry" [16], i.e., the system of equations must remain formally unchanged in regard to the change in the Lagrange variables. In what follows, while making some additional assumptions, we will construct a system of model equations that satisfies all of these requirements.

## III. MODEL

In this section, we construct a continuum paste model for a generic $n_d$-dimensional geometry. The model equations will be summarized at the end of Sec. III B. Subsequently, in Secs. IV and V, this model will be analyzed under a specific setup describing a two-dimensional slope flow with constant layer thickness. Readers who are more interested in the analysis than the model construction may, after checking Figs. 1 and 2, skip to Eqs. (44a)–(44c) at the end of Sec. IV.

### A. Kinematics

First, we review the Lagrangian description of kinematics. The configuration of an $n_d$-dimensional continuum is represented by a mapping from Lagrangian variable $\boldsymbol{\xi}$ (also known as "label" or "material variable" [16]) to the position vector $\mathbf{r}$. For $n_d = 3$, we write

$$\boldsymbol{\xi} = (\xi, \eta, \zeta) \mapsto \mathbf{r} = \mathbf{r}(\boldsymbol{\xi}, t) = \begin{bmatrix} x(\xi, \eta, \zeta, t) \\ y(\xi, \eta, \zeta, t) \\ z(\xi, \eta, \zeta, t) \end{bmatrix}_{\mathrm{C}}, \quad (5)$$

where $[\ ]_{\mathrm{C}}$ denotes the representation in terms of Cartesian components. For $n_d = 2$ we will omit $\eta$ and $y$, assuming that all the motion occurs in the $(x, z)$ plane.
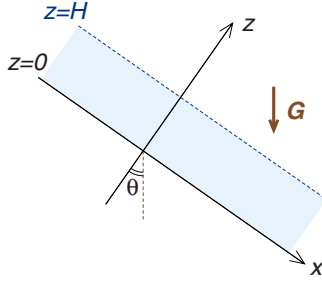
FIG. 2. (Color online) Schematic view of the system and coordinates. A uniform fluid layer with thickness $H$ is assumed. The label variable $\zeta$ coincides with the depthwise Eulerian coordinate $z$ in the present setup, and the velocity is $U\mathbf{e}_x$ where $U=\partial_t X(\zeta,t)$. The gravitational acceleration vector is $\mathbf{G}=(G\sin\theta)\mathbf{e}_x-(G\cos\theta)\mathbf{e}_z$, whose $x$ component is $G_x=G\sin\theta$.

The time derivative of $\mathbf{r}=\mathbf{r}(\boldsymbol{\xi},t)$ gives the velocity

$$\mathbf{v}=\partial_t\mathbf{r}(\boldsymbol{\xi},t). \qquad (6)$$

In Eq. (6) and in what follows, $\partial_t$ stands for the time derivative in the Lagrangian description (Lagrange derivative, which is usually denoted by $D/Dt$ in Eulerian description). Using $\{\partial_\xi\mathbf{r},\partial_\eta\mathbf{r},\partial_\zeta\mathbf{r}\}$ (where $\partial_i=\partial/\partial\xi^i$) as the set of local bases, we can represent the velocity as

$$\mathbf{v}=v^i\partial_i\mathbf{r}. \qquad (7)$$

In Eq. (7) and in what follows, summation over $i\in\{\xi,\eta,\zeta\}$ is understood according to Einstein's contraction rule. The coefficients $(v^i)$ in Eq. (7) are referred to as the contravariant components of $\mathbf{v}$ [see Eqs. (A1) and (A6) in Appendix A]. The acceleration is $\partial_t\mathbf{v}=\partial_t(v^i\partial_i\mathbf{r})$; we emphasize again that $\partial_t$ denotes the Lagrange derivative.

The square of the Euclidean distance between two neighboring "particles," labeled by $\boldsymbol{\xi}$ and $\boldsymbol{\xi}+d\boldsymbol{\xi}$, is

$$ds^2=|(\partial_i\mathbf{r})d\xi^i|^2=g_{ij}d\xi^i d\xi^j, \quad g_{ij}=(\partial_i\mathbf{r})\cdot(\partial_j\mathbf{r}), \qquad (8)$$

which introduces the metric tensor denoted by $(g_{ij})$ or $\mathbf{g}$. In this paper we refer to $\mathbf{g}$ as the "Euclidean" metric tensor, which does not mean that $g_{ij}$ is equal to Kronecker's delta but means that the Euclidean metric of the $\mathbf{r}$ space is imported into the $\boldsymbol{\xi}$ space by Eq. (8).

In general, it is totally unnecessary to choose $\boldsymbol{\xi}$ to be some "initial" position of the element, except for some particular situations in which the initial state has a special significance. One of these special cases is that of purely elastic bodies initially set in a stress-free and undeformed state, called a "natural state" [17]. It is meaningful in this case to choose the "natural state" position vector as $\boldsymbol{\xi}$ so that $g_{ij}$ defined by Eq. (8) is essentially identical to the Cauchy-Green deformation tensor [9] whose difference from $\delta_{ij}$ is responsible for the elastic restoring force. This is a rather special case, however. More generally, $\boldsymbol{\xi}$ has nothing to do with the initial state, and the *natural metric tensor* $\mathbf{g}^{\natural}$ is used as a reference to define the elastic deformation, instead of assuming the global existence of the stress-free natural state. The (locally) undeformed state is formulated as $\mathbf{g}=\mathbf{g}^{\natural}$, and the difference between $\mathbf{g}$ and $\mathbf{g}^{\natural}$ is responsible for the stress. More details about $\mathbf{g}^{\natural}$ will be discussed later.

The incompressibility condition is expressed as

$$\partial_t\det\mathbf{g}=0, \qquad (9)$$

because the mass of a fluid element is $\rho\sqrt{\det\mathbf{g}}\,d^{n_d}\boldsymbol{\xi}$ which should remain unchanged, and the density $\rho$ also remains unchanged during the motion. For simplicity, we assume that $\rho$ is a global constant. Then, without loss of generality, we can replace Eq. (9) by

$$\det\mathbf{g}=1. \qquad (10)$$

### B. Equation of motion and constitutive relation

Now we detail the dynamics. With the stress field denoted by $\mathbf{P}=P^{ij}(\partial_i\mathbf{r})\otimes(\partial_j\mathbf{r})$ and the external body force by $\mathbf{F}=F^i\partial_i\mathbf{r}$, the momentum equation is written as

$$\rho\partial_t(v^i\partial_i\mathbf{r})=-\frac{\partial}{\partial\mathbf{r}}\cdot{}^t[P^{ij}(\partial_i\mathbf{r})\otimes(\partial_j\mathbf{r})]+F^i\partial_i\mathbf{r}$$

or, in contravariant component representation, as [17]

$$\rho(\partial_t v^i+v^j\nabla_j v^i)=-\nabla_j P^{ij}+F^i. \qquad (11)$$

The left-hand side is the contravariant component of the acceleration vector $\partial_t\mathbf{v}$ multiplied by the density $\rho$, and $\nabla_j$ denotes the covariant derivative (these mathematical concepts are clarified in Appendix A to the degree sufficient for the present work; for a more profound understanding of the mathematical background, see Refs. [17,18]). While $\mathbf{F}$ is regarded as a given, $\mathbf{P}$ must be determined by a suitable constitutive relation.

From the discussion in the previous section, we expect that $\mathbf{P}$ obeys a viscoelastic equation of Maxwell type. The Maxwell model is often illustrated as a spring and dashpot connected in series [9], for which the relation between the tension $T$ and the total length $x$ is given by

$$T=\kappa(x_S-x_S^{\natural})=\mu\frac{dx_D}{dt}, \quad x=x_S+x_D, \qquad (12)$$

where $\kappa$ is the spring constant, $\mu$ is the resistance, $x_S$ and $x_D$ are the length of the spring part and the dashpot part, respectively, and $x_S^{\natural}$ denotes the natural length of the spring part. It is customary to eliminate the "internal" variables ($x_S$, $x_D$, and $x_S^{\natural}$) from Eq. (12), which yields

$$\left(\mu^{-1}+\kappa^{-1}\frac{d}{dt}\right)T=\frac{dx}{dt}. \qquad (13)$$

A time scale $\mu/\kappa$ in regard to stress relaxation is recognized in Eq. (13).

Now it is necessary to elaborate the Maxwell model in two respects: it needs to include plasticity and it also needs to describe $n_d$-dimensional continuum mechanics. In regard to the first point, most of the existing studies are based on an elastoplastic decomposition, which is a direct extension of Eq. (12). However, this approach has a disadvantage in that the incautious use of internal variables can lead to a difficulty, in particular for a finite deformation [19,20]. Here we adopt a different approach that is closer to Eq. (13), thereby

avoiding a direct reference to the internal variable $x_D$.

The essential idea is to attribute the relaxation to the natural length $x^\natural$, which is related to the tension $T$ as if the model is totally elastic:

$$T = \kappa(x - x^\natural). \tag{14}$$

The natural length $x^\natural$ can be expressed as $x^\natural = x_S^\natural + x_D$ in terms of internal variables, but this relation is not to be used explicitly; we note only that $x^\natural$ is time dependent while $x_S^\natural$ is not. By substituting Eq. (14) into Eq. (13), we find an equation that describes the relaxation of the natural length $x^\natural$:

$$\frac{dx^\natural}{dt} = \frac{\kappa}{\mu}(x - x^\natural), \tag{15a}$$

or, by introducing $\tau = \mu / \kappa$, as

$$\left(1 + \tau\frac{d}{dt}\right)x^\natural = x \tag{15b}$$

in the form of relaxation toward $x^\natural = x$. Equations (14), (15a), and (15b) provide us with a prototype of the plastic model.

Let us find $n_d$-dimensional continuum equations corresponding to the prototypical Eqs. (14), (15a), and (15b). As a candidate, we adopt an elastic constitutive equation

$$P^{ij} = \tilde{p}g^{ij} + S(g^{ij} - g_\natural^{ij}) \tag{16}$$

together with an inelastic equation

$$\partial_t g_\natural^{ij} = -\nu g_\natural^{ij} + \nu_* g^{ij}, \tag{17}$$

where $(g^{ij})$ denotes the inverse of the component matrix of the "Euclidean" metric tensor $(g_{ij})$, and $(g_\natural^{ij})$ is that of the natural metric tensor, such that

$$g_{ij}g^{jk} = g_{ij}^\natural g_\natural^{jk} = \delta_i^k.$$

The natural metric tensor $\mathbf{g}^\natural$ represents the square of the "natural distance" between two neighboring points labeled by $\boldsymbol{\xi}$ and $\boldsymbol{\xi} + d\boldsymbol{\xi}$,

$$(ds^\natural)^2 = g_{ij}^\natural d\xi^i d\xi^j, \tag{18}$$

in the sense that the difference between $ds^2$ and $(ds^\natural)^2$ accounts for the restoring force according to Eq. (16). In the special case of purely elastic bodies initially set in a stress-free "natural state" (at $t = t_0$), $ds^\natural$ is the distance in this initial configuration and $\mathbf{g}^\natural$ is the corresponding metric:

$$g_{ij}^\natural = g_{ij}|_{t=t_0} \quad \text{(purely elastic case)}.$$

In general, however, $\mathbf{g}^\natural$ differs from the initial value of $\mathbf{g}$. This is inevitable due to Eq. (17), which prescribes that the natural metric $\mathbf{g}^\natural$ is subject to relaxation. To make Eq. (17) more easily recognizable as a relaxation equation, we rewrite it in the manner of Eqs. (2) and (15b) as

$$(1 + \tau\partial_t)g_\natural^{ij} = Kg^{ij}, \quad \tau = \nu^{-1}, \quad K = \frac{\nu_*}{\nu}; \tag{19}$$

this equation provides that $(g_\natural^{ij})$ should evolve toward an isotropic tensor $(Kg^{ij})$. Plasticity is incorporated via $\tau$ according to Eq. (1). The idea of using a natural metric to reformulate the Maxwell model has been known among several researchers of rheology (including the authors of Refs. [11,12]), but the present author could not identify any publications in which the notion of the natural metric and its relaxation is formulated explicitly.

The $n_d$-dimensional elastic Eq. (16), corresponding to the one-dimensional Hookian Eq. (14), originates from consideration of elastic strain energy. Since $g_{ij}^\natural d\xi^i d\xi^j$ is a positive definite quadratic form, there exists a set of Euclidean vectors $\{\mathbf{p}_\xi, \mathbf{p}_\eta, \mathbf{p}_\zeta\}$ such that $g_{ij}^\natural = \mathbf{p}_i \cdot \mathbf{p}_j$ (this is proved essentially in the same way as the polar decomposition theorem [9,17]). Then, by defining

$$d\mathbf{r}^\natural = \mathbf{p}_i d\xi^i, \tag{20}$$

we have $(ds^\natural)^2 = d\mathbf{r}^\natural \cdot d\mathbf{r}^\natural = |d\mathbf{r}^\natural|^2$. Note that Eq. (20) does not claim that $d\mathbf{r}^\natural$ is a differential of "$\mathbf{r}^\natural$": such integrability is not guaranteed. However, it is legitimate to interpret $d\mathbf{r}^\natural$ as a natural configuration of each small element. Since $\mathbf{p}_i$'s must be linearly independent due to the positivity of det $\mathbf{g}^\natural$, Eq. (20) can be inverted, which we denote as $d\xi^i = \mathbf{p}_*^i \cdot d\mathbf{r}^\natural$. From this and the "Euclidean" metric (8), we have a relation between the Euclidean distance $ds$ and the natural configuration $d\mathbf{r}^\natural$,

$$ds^2 = (g_{ij}\mathbf{p}_*^i \otimes \mathbf{p}_*^j):(d\mathbf{r}^\natural \otimes d\mathbf{r}^\natural). \tag{21}$$

Let us denote the eigenvalues of this quadratic form by $\{\lambda_\alpha^2\}$ so that $ds^2 = \lambda_\alpha^2|d\mathbf{r}^\natural|^2$ along the $\alpha$th principal axis. The geometrical meaning of $\lambda_\alpha$ is clear: it represents the elongation factor of the line element. Isotropy requires that the elastic energy (denoted by $E$) should consist of a symmetric combination of these eigenvalues. The simplest form with a correct Hookian limit is

$$E = \frac{1}{2}S(\lambda_1^2 + \lambda_2^2 + \lambda_3^2 - 3) \tag{22}$$

for $n_d = 3$. Equation (22) is known as the neo-Hookian constitutive equation [17]. With the aid of the incompressibility condition, which implies $\lambda_1\lambda_2\lambda_3 = 1$, Eq. (22) reduces to $E = S(e_1^2 + e_2^2 + e_3^2)$ for small deformations ($\lambda_\alpha = 1 + e_\alpha$ and $|e_\alpha| \ll 1$). By using the definition of $\mathbf{p}_*^i$ and introducing $\varepsilon = \Sigma_\alpha(\lambda_\alpha^2 - 1)$, for finite deformations, the elastic energy $E$ is expressed in terms of the inverse natural metric tensor:

$$E = \frac{1}{2}S\varepsilon, \quad \varepsilon = g_{ij}g_\natural^{ij} - n_d. \tag{23}$$

By calculating the variation of the elastic energy $E$ in regard to $\mathbf{r}$ through the metric tensor $\mathbf{g}$ under the constraint of incompressibility condition (10), we find that the contravariant components of the stress tensor are given by Eq. (16). Details of this calculation are shown in Appendix B. Note that the tensor $(g^{ij})$ in the first term of the right-hand side of Eq. (16) stands for the Euclidean unit tensor:

$$g^{ij}(\partial_i\mathbf{r}) \otimes (\partial_j\mathbf{r}) = \mathbb{1}. \tag{24}$$

Thus we find that the term $\tilde{p}g^{ij}$ stands for an isotropic stress. The scalar $\tilde{p}$ is related to the hydrostatic pressure arising as a constraint force (Lagrange multiplier) for incompressibility. It is convenient to define

$$\overleftrightarrow{\sigma} = S[g^{ij}_{\natural}(\partial_i \mathbf{r}) \otimes (\partial_j \mathbf{r}) - \mathbb{1}] \qquad (25)$$

and call it the "elastic stress tensor" so that the stress tensor $\mathbf{P} = P^{ij}(\partial_i \mathbf{r}) \otimes (\partial_j \mathbf{r})$ is given by

$$\mathbf{P} = \tilde{p}\mathbb{1} - \overleftrightarrow{\sigma}. \qquad (26)$$

It is easy to confirm that $\overleftrightarrow{\sigma}$ vanishes when $g^{\natural}_{ij} = g_{ij}$.

We emphasize that $(g^{ij}_{\natural})$ in Eq. (25), which determines the elastic stress tensor $\overleftrightarrow{\sigma}$, is the *inverse* of the natural metric tensor. This must be the case so that $\overleftrightarrow{\sigma}$ should remain invariant under the relabeling of the Lagrange variables. This is also acceptable if we remember that springs with different lengths but the same local properties obey a constitutive relation analogous to Eq. (25),

$$T = s_0 \left( \frac{x}{x^{\natural}} - 1 \right),$$

where $s_0$ is the normalized spring constant, and notice that $\overleftrightarrow{\sigma}$ is an intensive variable as well as the tension $T$ and therefore must be expressed as such.

Now we discuss the inelastic part of our model described by Eq. (17). This equation states the relaxation of the inverse natural metric tensor, formulated according to the following discussion on interparticulate bonds. The natural metric represents the energetically optimal configuration of the particles determined by the bond network. The network strength, or the bond density, is represented by the inverse natural metric $\mathbf{g}_{\natural}$ (not by the natural metric $\mathbf{g}^{\natural}$ itself). In flowing pastes, however, this bond network is ephemeral. We suppose that the network is destroyed at some rate and reconstructed isotropically. With the destruction rate denoted by $\nu$ and the reconstruction rate by $\nu_*$, the temporal change of the bond density is given by $-\nu g^{ij}_{\natural} + \nu_* g^{ij}$, leading to Eq. (17).

The ratio $K = \nu_* / \nu$ is determined by postulating the incompressibility of $\mathbf{g}^{\natural}$,

$$\det \mathbf{g}^{\natural} = 1. \qquad (27)$$

Differentiating Eq. (27) with regard to $t$ and then substituting Eq. (17) into it, we find that $n_d \nu = g^{\natural}_{ij} g^{ij} \nu_*$, which implies

$$K = \frac{n_d}{g^{\natural}_{ij} g^{ij}} \quad \left( \text{i.e.,} \quad \nu_* = \frac{n_d}{g^{\natural}_{ij} g^{ij}} \nu \right). \qquad (28)$$

According to Eq. (1) in the previous section, $\tau$ is supposed to be a function of the elastic strain energy, so that $\tau = \tau(\varepsilon)$ with $\varepsilon$ given by Eq. (23). The simplest form consistent with Eq. (1) is

$$\tau = \begin{cases} +\infty & (\varepsilon < \sigma_Y^2 / S^2) \\ \eta_p / S & (\varepsilon > \sigma_Y^2 / S^2), \end{cases}$$

where $\sigma_Y$ is the yield stress (we will see later that the energy $\varepsilon$ for shear stress $\sigma$ is calculated to be $\sigma^2 / S^2$). It is physically more realistic and mathematically less problematic to suppose that $\tau$ is a continuous function of $\varepsilon$. Here we assume

$$\tau = \nu^{-1}, \quad \nu = \nu(\varepsilon) = \frac{S}{\eta_p} \max\left( 0, 1 - \frac{\sigma_Y / S}{\sqrt{\varepsilon}} \right), \qquad (29)$$

which is Lipschitz-continuous in spite of weak singularity at the yield point (Fig. 1). Equation (29) is chosen in such a way that it agrees with Bingham plasticity [13,21,22] for simple shear flow with shear rate $\dot{\gamma}$, where the shear stress $\sigma$ is estimated to be $\sigma \simeq S \tau \dot{\gamma}$. Admitting $\varepsilon \simeq \sigma^2 / S^2$, from Eq. (29) we find

$$\dot{\gamma} \simeq \frac{\nu \sigma}{S} = \nu(\varepsilon) \sqrt{\varepsilon} = \begin{cases} 0 & (\varepsilon < \sigma_Y^2 / S^2) \\ \eta_p^{-1}(S\sqrt{\varepsilon} - \sigma_Y) & (\varepsilon > \sigma_Y^2 / S^2), \end{cases}$$

which is Bingham plasticity.

Let us summarize our model. The governing system of equations consists of Eqs. (11), (16), (19), and (29), supplemented with the kinematic relations (6)–(8), as well as incompressibility conditions (10) and (27). Equation (29) requires the evaluation of $\varepsilon$ by Eq. (23), which is actually not independent of Eq. (16), but should be included in the model for convenience. The independent variables are $\xi$ and $t$ (Lagrangian description), and the essential dependent variables are $\mathbf{r}$ and $\mathbf{g}^{\natural}$. The velocity and the Euclidean metric tensor are derived from the differentials of $\mathbf{r} = \mathbf{r}(\xi, t)$. Due to the incompressibility condition, there arise two additional scalar fields, namely, $\tilde{p}$ and $K$; the latter is determined by Eq. (28).

### C. Navier-Stokes limit

There remains the task to confirm that the whole system of model equations reduces to the $n_d$-dimensional incompressible Navier-Stokes equation if $\tau$ is set to be a small constant such that $\tau \ll \|\nabla \mathbf{v}\|^{-1}$. By expanding $g^{\natural}_{ij}$ (as well as $g^{ij}_{\natural}$) and $K$ in power series of $\tau$, from Eqs. (19) and (27) we find

$$g^{ij}_{\natural} = g^{ij} - \tau \partial_t g^{ij} + O(\tau^2), \quad K = 1 + O(\tau^2). \qquad (30)$$

The time-derivative term $\partial_t g^{ij}$ on the right-hand side of Eq. (30) is calculated as

$$\partial_t g^{ij} = -g^{ik} g^{jl} \partial_t g_{kl} \qquad (31a)$$

and

$$\partial_t g_{ij} = \partial_t[(\partial_i \mathbf{r}) \cdot (\partial_j \mathbf{r})] = (\partial_i \mathbf{v}) \cdot (\partial_j \mathbf{r}) + (\partial_i \mathbf{r}) \cdot (\partial_j \mathbf{v})$$
$$= \nabla_i v_j + \nabla_j v_i, \qquad (31b)$$

where $(v_i)$ denotes the covariant components of the velocity vector $\mathbf{v}$, and $\nabla_i v_j$ denotes the covariant derivative of $v_j$ defined by $\partial_i(v_j \nabla \xi^j) = (\nabla_i v_j) \nabla \xi^j$. Using Eqs. (31a) and (31b) to evaluate $g^{ij}_{\natural}$ in Eq. (30), from Eq. (25) we obtain

$$\overleftrightarrow{\sigma} = S[g^{ij}_{\natural}(\partial_i \mathbf{r}) \otimes (\partial_j \mathbf{r}) - \mathbb{1}]$$
$$= S(g^{ij}_{\natural} - g^{ij})(\partial_i \mathbf{r}) \otimes (\partial_j \mathbf{r}) = -S\tau(\partial_t g^{ij})(\partial_i \mathbf{r}) \otimes (\partial_j \mathbf{r})$$
$$= S\tau(g^{ik} g^{jl} \partial_t g_{kl})(\partial_i \mathbf{r}) \otimes (\partial_j \mathbf{r}) = S\tau(\partial_t g_{kl})(\nabla \xi^k) \otimes (\nabla \xi^l)$$
$$= S\tau(\nabla_k v_l + \nabla_l v_k)(\nabla \xi^k) \otimes (\nabla \xi^l) = S\tau[\nabla \otimes \mathbf{v} + {}^t(\nabla \otimes \mathbf{v})],$$

and identify it with the Newtonian-Stokesian relation

$$\vec{\sigma} = 2\eta_* \text{ sym grad } \mathbf{v} \quad (\eta_* = S\tau), \tag{32}$$

where sym grad $\mathbf{v}$ denotes the symmetric part of $\nabla \otimes \mathbf{v}$. The equation of motion then reduces to the Navier-Stokes equation, which was to be demonstrated.

## IV. SIMPLIFICATION FOR SLOPE FLOWS WITH UNIFORM THICKNESS

We have obtained a system of equations that is acceptable as a model of isotropic pastes. Next, let us analyze this system under a particular setup describing slope flows. Though the equations are $n_d$-dimensional and it is also possible to formulate boundary conditions for fully three-dimensional surface deformations, it is not wise trying to solve the full system immediately by direct numerical simulations, as it would require too much difficulty and provide too little insight. Rather, the first thing to do is to elucidate the basic behavior of the model in the simplest situation.

Here, we study a two-dimensional paste flow ($n_d=2$) on a slope inclined by an angle $\theta$. The setup of the system is shown in Fig. 2. All of the motion is supposed to occur in the $(x, z)$ plane, and it is in this plane that the paste is assumed to be isotropic. The flow is driven by the gravitational force $\mathbf{F} = \rho\mathbf{G}$, where $\mathbf{G}$ is the gravitational acceleration vector,

$$\mathbf{G} = \begin{bmatrix} G\sin\theta \\ -G\cos\theta \end{bmatrix}_\text{C} = (G\sin\theta)\mathbf{e}_x - (G\cos\theta)\mathbf{e}_z. \tag{33}$$

The free surface requires the dynamical boundary condition and the kinematic boundary condition. The dynamical boundary condition prescribes the continuity of the stress, while the kinematic boundary condition postulates that the surface must move together with the adjacent fluid to satisfy the mass conservation law. Since we assume here that the paste layer has a constant thickness $H$, the dynamical boundary condition reduces to $P^{ij}\nabla_j z = 0$ [see Eq. (A20) and the text below it in Appendix A]. The kinematic boundary condition is trivially satisfied by assuming that the velocity field is also uniform in regard to $x$ and parallel to the $x$ axis.

Under the present assumptions, the fluid motion is expressed in terms of a single function which we denote by $X = X(\zeta, t)$, as

$$\mathbf{r} = \begin{bmatrix} \xi + X \\ \zeta \end{bmatrix}_\text{C} = (\xi + X)\mathbf{e}_x + \zeta\mathbf{e}_z. \tag{34}$$

The time derivative of Eq. (34) gives the velocity

$$\mathbf{v} = \partial_t \mathbf{r} = U\mathbf{e}_x, \tag{35}$$

where $U = \partial_t X$. By substituting Eq. (34) into Eq. (8), we obtain the Euclidean metric tensor $g_{ij}$ expressed in terms of $X$,

$$\mathbf{g} = \begin{bmatrix} g_{\xi\xi} & g_{\xi\zeta} \\ g_{\zeta\xi} & g_{\zeta\zeta} \end{bmatrix} = \begin{bmatrix} 1 & X' \\ X' & 1 + X'^2 \end{bmatrix}, \tag{36}$$

where $X'$ is an abbreviation for $\partial X/\partial\zeta$. The incompressibility condition (10) is already satisfied and there is no need to require it particularly.

Let us concretize the equations containing the natural metric. The calculation can be performed in at least two dif-

ferent ways: one may evaluate the terms in the momentum equation (11) either on the ground of modern differential geometry of the Riemannian manifold determined by $g_{ij}$, or fully utilizing the Cartesian components in the embedding Euclidean space, as is shown in the latter half of Appendix A. Both methods yield the same result.

As the natural metric tensor for the present case is a 2 $\times$ 2 symmetric tensor with det $\mathbf{g}^\natural$ fixed to be unity, it can be expressed by two parameters. We set

$$\mathbf{g}^\natural = \begin{bmatrix} g_{\xi\xi}^\natural & g_{\xi\zeta}^\natural \\ g_{\zeta\xi}^\natural & g_{\zeta\zeta}^\natural \end{bmatrix} = \begin{bmatrix} e^{-\alpha} & \beta \\ \beta & (1+\beta^2)e^\alpha \end{bmatrix}, \tag{37}$$

with $\alpha = \alpha(\zeta, t)$, $\beta = \beta(\zeta, t)$, and calculate its inverse matrix $\mathbf{g}_\natural$. Then we substitute it, together with $\mathbf{g}^{-1}$ calculated from Eq. (36), into the equations composing the constitutive relation. Equation (16) then yields the stress tensor $\mathbf{P}$. Its Cartesian representation, calculated from Eqs. (25) and (26), reads

$$\mathbf{P} = \tilde{p}\mathbb{1} - \vec{\sigma} = \tilde{p}\mathbb{1} - S \begin{bmatrix} e^\alpha(1+\tilde{\sigma}^2) - 1 & \tilde{\sigma} \\ \tilde{\sigma} & e^{-\alpha} - 1 \end{bmatrix}_\text{C}, \tag{38}$$

where $\tilde{\sigma} = \sigma_{xz}/S$ stands for the nondimensionalized shear stress, and is given by

$$\tilde{\sigma} = e^{-\alpha}X' - \beta. \tag{39}$$

The momentum equation (11) reads

$$\rho\partial_t U = S\partial_\zeta\tilde{\sigma} + \rho G_x, \tag{40}$$

where $G_x = G\sin\theta$ is the $x$-directional component of the gravitational acceleration vector $\mathbf{G}$, given by Eq. (33). Note that the depthwise component of the equation of motion does not participate in the dynamics, as it determines only the hydrostatic pressure.

From Eq. (17) or (19), taking Eq. (28) into account and using $\mathbf{g}$ parametrized as Eq. (36) and $\mathbf{g}^\natural$ as Eq. (37), we obtain

$$\tau\partial_t\alpha = 1 - \frac{2}{2+\varepsilon}e^\alpha, \tag{41}$$

$$\tau\partial_t\beta = -\beta + \frac{2}{2+\varepsilon}X', \tag{42}$$

where we have utilized the relation $K = 2/(2+\varepsilon)$ with $\varepsilon$ defined by Eq. (23), which holds for the two-dimensional case (we note that the three-dimensional case is not so simple). By calculating $\varepsilon$ from Eq. (23) and then rewriting the result in terms of $\tilde{\sigma}$, we find

$$\varepsilon = e^\alpha(e^{-\alpha}X' - \beta)^2 + 2(\cosh\alpha - 1) = e^\alpha\tilde{\sigma}^2 + 2(\cosh\alpha - 1). \tag{43}$$

Note that Eq. (43) endorses the relation between $\varepsilon$ and $\tilde{\sigma}$ stated several lines before Eq. (29), as long as $\alpha = o(\tilde{\sigma})$ (which is usually the case).

Though the above equations constitute a closed system, $X'$ and $\beta$ are inconvenient variables as they increase unboundedly as time elapses. To avoid this inconvenience, we rewrite the equations in terms of $U$ and $\tilde{\sigma}$. Using the evolu-

tion of $\tilde{\sigma}$ instead of Eq. (42) for $\beta$, and also rewriting $\tau$ in terms of $\nu(\varepsilon)$, we obtain a system of three equations governing three variables, namely, $\alpha(\zeta, t)$, $\tilde{\sigma}(\zeta, t)$, and $U(\zeta, t)$:

$$\partial_t \alpha = \nu(\varepsilon)\left(1 - \frac{2e^\alpha}{2 + \varepsilon}\right), \tag{44a}$$

$$\partial_t \tilde{\sigma} = e^{-\alpha}\partial_\zeta U - \nu(\varepsilon)\tilde{\sigma}, \tag{44b}$$

$$\partial_t U = \frac{S}{\rho}\partial_\zeta \tilde{\sigma} + G_x. \tag{44c}$$

Aside from the curious Eq. (44a) for $\alpha$, this system of equations has a familiar form that can be recognized as a description of a slope flow (Fig. 2), with Eq. (44b) relating the nondimensional shear stress $\tilde{\sigma}$ to the shear rate $\partial_\zeta U$, and Eq. (44c) describing momentum balance. Plasticity is introduced via $\nu(\varepsilon)$, that is, the inverse of the relaxation time mentioned in Eq. (1). The functional form of $\nu(\varepsilon)$ is specified by Eq. (29) and Fig. 1 on the basis of Bingham plasticity. The nondimensional strain energy $\varepsilon$, defined by Eq. (23), is evaluated as a function of $\tilde{\sigma}$ and $\alpha$ as in Eq. (43).

Equations (44a)–(44c) require two boundary conditions. We pose a no-slip boundary condition at the wall,

$$U|_{\zeta=0} = 0, \tag{45}$$

while the free-surface condition, for the present case, gives

$$\tilde{\sigma}|_{\zeta=H} = 0. \tag{46}$$

## V. ANALYSIS

### A. Qualitative consideration

Equations (44a)–(44c) together with two boundary conditions define a closed system of evolutional equations. The energy is supplied by gravitational work $\rho G_x U$, stored as elastic energy $\varepsilon$, and dissipated through the relaxation of $\mathbf{g}^\natural$ that represents the viscous part of the Maxwell model. Plasticity implies that the dissipation process is limited by a threshold, in such way that the relaxation time can become infinitely large according to Eq. (29). This allows some part of the elastic energy to remain frozen inside the paste.

In the present study, $\alpha$ plays an important role. Equation (44a) clarifies that the threshold mechanism included in $\nu(\varepsilon)$, shown in Fig. 1, governs the fundamental behavior of $\alpha$. For an $\varepsilon$ smaller than the threshold value, $\nu(\varepsilon)$ vanishes and therefore a practically arbitrary function of $\zeta$ is admissible as a steady solution to Eq. (44a), as long as it allows $\varepsilon$ to stay within the threshold. This implies a strong nonuniqueness of $\alpha$ that can remain in the static paste; there is an infinitely large number of possibilities, whose realization depends on the time-dependent process of evolution (an analogous situation occurs also in dry granular materials subject to static friction [23]). On the other hand, $\alpha$ in the flowing paste is expected to evolve toward a steady solution that is uniquely determined if the external force, layer thickness, and paste properties are specified. This steady solution will be provided later in a closed form.

We will show that the residence of an $\alpha > 0$ in the paste means the presence of $x$-directional tension. Then we will derive a steady solution for a flowing paste analytically, showing that $\alpha$ is positive there. Time-dependent numerical calculations for flowing pastes typically exhibit relaxation toward this solution, involving the creation of a positive $\alpha$. The numerical calculations also show that some portion of $\alpha$ remains in the paste after its flow is stopped, and the residual value of $\alpha$ is still positive. This process creates an $x$-directional tension remaining in the paste and therefore gives a possible clarification of the type-I Nakahara effect.

### B. Residual tension

Let us confirm that $\alpha > 0$ implies tension. This is intuitively evident if we recall that $e^{-\alpha}$ stands for the $\xi\xi$ component of the natural metric tensor (37), and conceive of $e^{-\alpha} < 1$ as contraction of natural length of the (supposed) "springs" in the $x$ direction. More formally, this is demonstrated by calculating the normal stress difference for the "ground state" that minimizes the elastic energy $\varepsilon$ as a function of $\mathbf{g}$, with $\mathbf{g}^\natural$ being fixed. In terms of the parametrization given by Eqs. (36) and (37), the problem is to minimize $\varepsilon = \varepsilon(X', \alpha, \beta)$ for fixed values of $(\alpha, \beta)$.

From Eq. (43) we find that the minimizer of $\varepsilon(X', \alpha, \beta)$ is $X' = e^\alpha \beta$, or equivalently $\tilde{\sigma} = 0$ (vanishing shear stress). Then, using Eq. (38) to calculate the diagonal components of $\overleftrightarrow{\sigma}$ in Eq. (25), we find the normal stress difference

$$\sigma_{xx} - \sigma_{zz} = 2S \sinh \alpha \tag{47}$$

for $\tilde{\sigma} = 0$. Clearly, this is positive for $\alpha > 0$, showing a residual tension in the $x$ direction.

### C. Steady solution for flowing pastes

Equation (47) shows that a paste layer left in the unloaded state ($\tilde{\sigma} = 0$) bears an $x$-directional tension if $\alpha > 0$. The next task is to show that the flow makes $\alpha > 0$ if it approaches a steady solution of Eqs. (44a)–(44c).

For steady flows, the nondimensional shear stress $\tilde{\sigma} = \sigma_{xz}/S$ is determined by the momentum balance (44c) and the free surface boundary condition (46). The result is

$$\tilde{\sigma} = \frac{\rho G_x}{S}(H - \zeta). \tag{48}$$

Note that Eq. (48) holds for *static* states as well. For that case, the steady solution consists of Eq. (48), $U = 0$, and an arbitrary $\alpha = \alpha(\zeta)$ such that $\varepsilon < \sigma_Y^2/S^2$ [i.e., $\nu(\varepsilon) = 0$]. On the other hand, $\nu(\varepsilon)$ must be nonzero for *flowing* pastes, which makes the steady solution totally different. For steady flows [$\nu(\varepsilon) \neq 0$ and $\partial_t \alpha = 0$], Eq. (44a) yields

$$\varepsilon = 2(e^\alpha - 1). \tag{49}$$

Since $\varepsilon$ must be positive according to Eq. (43), from the above Eq. (49) it follows that $\alpha$ must be positive as well. More concretely, from Eqs. (43), (48), and (49) we find

$$\alpha = -\frac{1}{2}\ln(1 - \tilde{\sigma}^2) = -\frac{1}{2}\ln\left[1 - \left(\frac{\rho G_x}{S}(H - \zeta)\right)^2\right] \quad (50)$$

for the flowing part of the paste in steady state. It is also confirmed that $\varepsilon \simeq \tilde{\sigma}^2$ for small $|\tilde{\sigma}|$.

The neighborhood of the free surface requires a separate treatment, because this region remains solidified due to the lack of a sufficient shear stress. The boundary between the solidified and fluidized regions can be calculated by using Eqs. (49) and (50), which give $\varepsilon = \varepsilon[\alpha(\zeta)]$ in the fluidized region, to find the location $\zeta_Y$ such that $\varepsilon[\alpha(\zeta_Y)] = \sigma_Y^2/S^2$. In the region $\zeta_Y < \zeta < H$ where the paste is solidified, the velocity $U$ is uniform. The velocity $U$ in the fluidized region can be obtained by integrating Eq. (44b) under the boundary condition (45).

As is evident from Eq. (48), the maximum of the shear stress $\sigma_{xz}$ occurs at the wall. The wall shear stress and its nondimensionalized value are $\sigma_{xz}|_{\zeta=0} = \rho G_x H$ and $\tilde{\sigma}|_{\zeta=0} = \rho G_x H/S$. For the paste to flow steadily, this wall shear stress $\rho G_x H$ must be greater than the yield stress $\sigma_Y$. The maximum $\alpha$ also occurs at the wall:

$$\max_\zeta \alpha = -\frac{1}{2}\ln\left[1 - \left(\frac{\rho G_x H}{S}\right)^2\right] \quad (51)$$

according to Eq. (50).

The above discussion suggests two nondimensional parameters that can be expressed as a ratio $\rho G_x H : \sigma_Y : S$. Let us complete the dimensional analysis of Eqs. (44a)–(44c) before proceeding to the numerical calculation of time-dependent solutions.

### D. Dimensional analysis

Equations (44a)–(44c) contain five physical parameters, namely, $S$, $\eta_p$, $\rho$, $G_x$, and $\sigma_Y$ (the last one comes through $\nu$). The first three determine the viscoelastic time scale $\tau_0 = \eta_p/S$ and the length scale $\ell_0 = \eta_p/\sqrt{\rho S}$. The boundary conditions introduce the layer thickness $H$ as another length scale.

The system is characterized by three nondimensional parameters, for example, $H/\ell_0$, $\sigma_Y/S$, and $\rho G_x H/S$ (or a suitable combination of them). Note that $\rho G_x H$ gives an estimation of the wall shear stress, which represents the magnitude of the external forcing.

Evaluation of Reynolds number will be useful for considering the Newtonian limit. On the basis of $\eta_p$, $H$, and $U \sim \rho G_x H/(\eta_p/H) = \rho G_x H^2/\eta_p$, it is estimated as

$$R_H \sim \left(\frac{H}{\ell_0}\right)^2 \frac{\rho G_x H}{S};$$

this is indeed calculated from two of the three parameters stated above. In the present setup, $H$ is taken as the representative length scale, but we point out a general possibility that the system may be characterized by other Reynolds numbers, such as $R_L = UL/\eta_p$ based on the horizontal length scale $L$. In future studies this point may have to be taken into account.
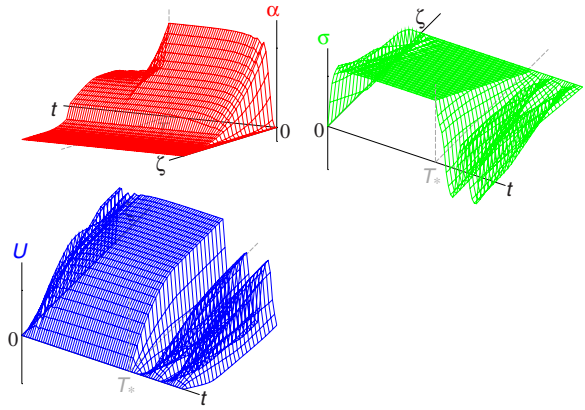


FIG. 3. (Color online) Typical evolution of $(\alpha, \tilde{\sigma}, U)$.

### E. Numerical calculation of unsteady solution

The author calculated the numerical solutions of Eqs. (44a)–(44c) (slightly modified, as we will see below) under the initial condition $(\alpha, \tilde{\sigma}, U)|_{t=0} = (0,0,0)$ and the boundary conditions (45) and (46), with $\nu[\varepsilon(\alpha, \tilde{\sigma})]$ defined by Eqs. (29) and (43), for hundreds of different nondimensional parameters. With the hyperbolic character of Eqs. (44a)–(44c) taken into account, the calculation adopted the two-step Lax-Wendroff scheme [24].

Since we are interested not only in the creation process of $\alpha$, but also the storage of $\alpha$ after the flow is stopped, it is necessary to simulate the process to stop the flow. To this aim, we "switch off" gravity at some time $t = T_*(\gg \tau_0)$, replacing Eq. (44c) by

$$\partial_t U = \frac{S}{\rho}\partial_\zeta \tilde{\sigma} + \frac{F_x}{\rho}, \quad F_x = \begin{cases} \rho G_x & (0 < t < T_*) \\ 0 & (t > T_*) \end{cases} \quad (52)$$

with $T_* = 100\tau_0$ or $T_* = 200\tau_0$.

Figure 3 depicts a typical evolution of $(\alpha, \tilde{\sigma}, U)$. The parameters are $H = 5\ell_0$, $\rho G_x H : \sigma_Y : S = 0.6 : 0.3 : 1$, and $T_* = 100\tau_0$. In the first stage of the evolution, the system rapidly approaches steady state, except for the region adjacent to the boundary between the fluidized and solidified regions ($\zeta = \zeta_Y = 2.58\ell_0$) where the relaxation time is significantly longer. After the gravity is "switched off" at $t = T_*$, both $\tilde{\sigma}$ and $U$ oscillates around zero. This oscillation should be damped if we consider the solvent viscosity, which is neglected in the present model. What must be noted is that $\alpha$ remains finite, though it decreases, after the driving force is switched off at $t = T_*$. The sign of the residual $\alpha$ is positive.

According to the analysis of 801 cases with $T = 100\tau_0$ and 689 cases with $T = 200\tau_0$, the behavior of $\alpha$ for different values of $\rho G_x H$ is summarized as follows. For $\rho G_x H$ smaller than $\sigma_Y/2$, throughout the evolution $\alpha$ remains zero. If $\rho G_x H$ exceeds $\sigma_Y/2$ but still remains below $\sigma_Y$, the evolution during the forcing ($0 < t < T_*$) is basically unsteady, where $\alpha$ is produced little by little from the interference of the stress waves. For $\sigma_Y < \rho G_x H < S$ (we always assume $\sigma_Y < S$), steady yield flow occurs, creating $\alpha$ according to Eq. (50). In both regimes stated above, a residual $\alpha$ is observed after $t = T_*$. The steady solution, Eq. (50), ceases to exist for $\rho G_x H > S$, which leads to the unlimited acceleration of the
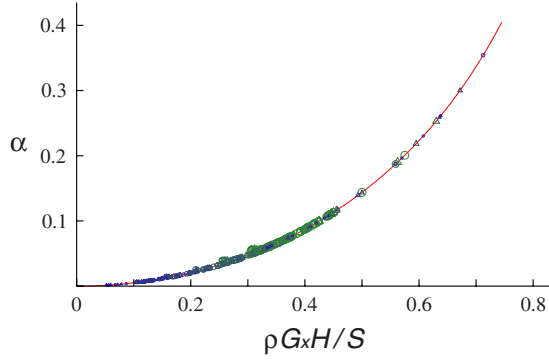
FIG. 4. (Color online) Steady values of $\alpha$ during the forcing. Spatial maximum of $\alpha$, whose steadiness is checked for a certain time range, is plotted against $\rho G_x H / S$. The line shows the analytical solution (51). The circles and the triangles represent numerical values for $T_* = 100\tau_0$ and $T_* = 200\tau_0$, respectively. The size and the color of the symbols indicate $\sigma_Y / S$, from the small blue symbols for $\sigma_Y = 0.05S$ to the large green symbols for $\sigma_Y = 0.30S$.

flow. This last case is out of the scope of the present model, because $U$ should be limited if, again, the solvent viscosity is taken into account.

Steady solutions obtained by the time-dependent calculation during the forcing, approximately for $T_*/2 < t < (3/4)T_*$, are checked against the analytical solution in Fig. 4. The curve shows $\max_\zeta \alpha$ given by Eq. (51) as a function of $\rho G_x H / S$. The symbols, consisting of 122 circles ($T_* = 100\tau_0$) and 110 triangles ($T_* = 200\tau_0$), indicate the numerical values of $\max_\zeta \alpha$ calculated within the range $\sigma_Y < \rho G_x H < 0.72S$, $0.05S \leq \sigma_Y \leq 0.30S$, and $0.20\ell_0 \leq H \leq 8.0\ell_0$. The size (and the color) of each symbol indicates the magnitude of $\sigma_Y / S$. Figure 4 demonstrates that the value of steady $\alpha$ is independent of $\sigma_Y$, once $\rho G_x H$ exceeds it. For $T_* = 100\tau_0$, there were several cases for which $\alpha$ did not attain its steady value (with the criterion $\Delta\alpha/|\alpha| = 0.02$); these cases are eliminated from Fig. 4 for clarity. Such exceptional cases did not occur for $T_* = 200\tau_0$.

As an explanation of the Nakahara effect, it is essential to show that some of $\alpha$ remains in the paste even after the flow is stopped, instead of decaying away. Figure 5 shows the numerical values of $\max_\zeta \alpha$ remaining steady (not to decay any more) after the flow is stopped. Here not $\alpha$ itself, but $\alpha S^2 / \sigma_Y^2$ is plotted against $\rho G_x H / \sigma_Y$ for $\rho G_x H > \sigma_Y/2$ (the ranges of $\sigma_Y / S$ is the same as in Fig. 4, and that of $H/\ell_0$ is $0.05\ell_0 \leq H \leq 8.0\ell_0$). The values of residual $\alpha$ for $\sigma_Y < \rho G_x H < 1.3\sigma_Y$ is fitted by

$$\max_\zeta \alpha \sim \frac{\sigma_Y^2}{S^2}\left(0.75\frac{\rho G_x H}{\sigma_Y} - 0.2\right). \tag{53}$$

In contrast to the steady value of $\alpha$ in the flow subject to the driving force, the residual value of $\alpha$ in Eq. (53) is strongly dependent on $\sigma_Y$. In particular, if $\rho G_x H / \sigma_Y$ is kept constant, Eq. (53) states that the residual value of $\alpha$ is scaled by $(\sigma_Y / S)^2$. This result seems understandable if we assume that, during the decay of $\alpha$ and $\tilde{\sigma} = \sigma_{xz}/S$, the first equal sign in Eq. (50) remains valid, until $\sigma_{xz}$ reaches the threshold value $\sigma_Y$. This gives a rough estimation of the residual $\alpha$
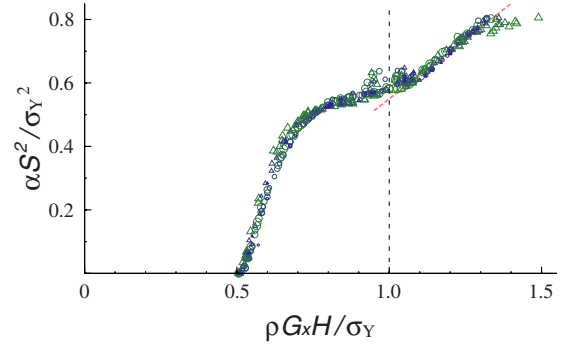


FIG. 5. (Color online) Residual value of $\alpha$ that remains in the paste after the forcing is removed. The spatial maximum of $\alpha$, rescaled by $(\sigma_Y / S)^2$, is plotted against $\rho G_x H / \sigma_Y$. The same symbols (circles and triangles) are used as in Fig. 4. The nonvertical broken line, with slope 0.75, represents the fitting relation (53).

$\simeq 0.5(\sigma_Y / S)^2$. Unfortunately, theoretical clarification of Eq. (53) in regard to its dependence on $\rho G_x H / \sigma_Y$ is not currently available.

## VI. DISCUSSION AND CONCLUDING REMARKS

### A. Relationship with crack pattern experiments

In this paper we have found the creation and fixation of the $x$-directional tension using a model equation for flows of isotropic pastes. This provides a possible scenario for the Nakahara effect (type I).

During the drying process, the paste slowly shrinks. Mathematically, this process is described as an isotropic contraction (shrinking) of the natural metric $\mathbf{g}^\natural$. If the paste had not undergone a flowing process, this contraction would produce a basically isotropic tension in the $(x, y)$ plane (parallel to the surface and the bottom) and therefore would lead to isotropic crack patterns. Actually, this is not the case: we have found that a positive $\alpha$ is created during the flowing process, which implies that the natural metric is already *contracted* in the streamwise direction. Strictly speaking, the present analysis is limited to the two-dimensional system in the $(x, z)$ plane and therefore it cannot tell whether any $y$-directional contraction occurs, but it is unlikely that it will occur to the same extent as the $x$-directional contraction. In fact, though a full analysis of three-dimensional system is too complicated to develop here, a simple perturbation analysis supports the above conjecture. The bonds parallel to the flow are therefore the first ones to break, causing cracks perpendicular to the flow and thus clarifying the Nakahara effect.

The present numerical analysis predicts that the magnitude of the residual $\alpha$ is scaled by $(\sigma_Y / S)^2$, as is seen in Fig. 5 and Eq. (53). This result is consistent with the observation of Nakahara and Matsuo in regard to the strength of the memory effect summarized as Fig. 2 in Ref. [3]. The figure presents a classification of the observed patterns as a function of the solid volume fraction (density of the paste) and the strength of the external forcing. Its region B, which lies just above the yield stress line and exhibits the memory effect, is subdivided according to the strength of the anisotropy
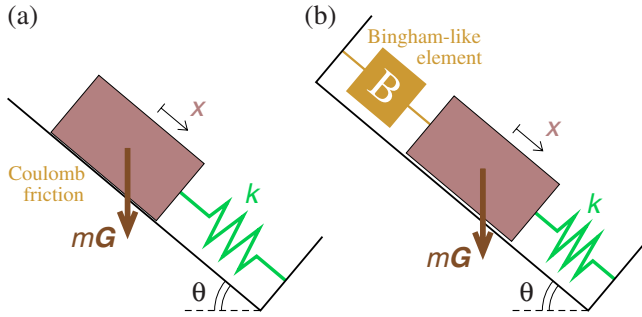
FIG. 6. (Color online) Duran's brick on a slope to illustrate static indeterminacy. (a) Original setup due to Duran [23]. Besides the gravity and the repulsion of the spring, the brick is subject to static Coulomb friction. (b) A modified setup, where Coulomb friction is replaced by a Bingham-like elastoplastic element.

in the pattern; strong anisotropy is observed for denser pastes (lamellar crack patterns, denoted by solid squares, occupy the subregion with volume fraction greater than 40%), while less dense pastes exhibit weaker anisotropy, resulting in large-scale lamellar cracks ($\gg H$) combined with cellular structure with smaller length scales ($\sim H$). If we admit that $\sigma_Y / S$ is greater for denser pastes, the difference in the strength of anisotropy can be explained from our theory predicting $\alpha \propto (\sigma_Y / S)^2$.

### B. Comparison with dry granular flows and other systems exhibiting memory effects

Memory effects are quite common in many glassy systems, ranging from granular matters to spin glasses. In the case of dry granular matters [23,25], history-dependent behavior essentially originates from the existence of interparticulate static friction. According to Coulomb's friction law, the interparticulate forces admit static indeterminacy, giving rise to the history-dependent stress state. Fluidization and solidification of granular matter also involves the creation and destruction of grain-scale structures, such as arching and force chains. Though the present study on paste flows is based on macroscopic description and therefore discussion on the grain-scale structure is outside its scope, comparative consideration on static indeterminacy is quite helpful in understanding some common mechanisms underlying paste flows and dry granular flows.

As seen at the top of Sec. V, the threshold mechanism in $\nu(\varepsilon)$ results in the static indeterminacy of $\alpha$. It is this static indeterminacy that enables the retention of the memory of the shear flow. (In a different setup [13], residual stress is introduced via static indeterminacy of $\beta$.) Thus the present paste model shares an important feature with dry granular systems.

To elucidate the analogy and distinction between the Bingham plasticity and Coulomb friction, let us consider an instructive problem taken from Chap. 3 of Duran's book [23]. Suppose a brick on an inclined wall, subject to static Coulomb friction (coefficient $\mu_s$) and a spring, as is illustrated in Fig. 6(a). Duran's problem is to determine the deformation $x$ (or equivalently the repulsion $kx$) of the spring as
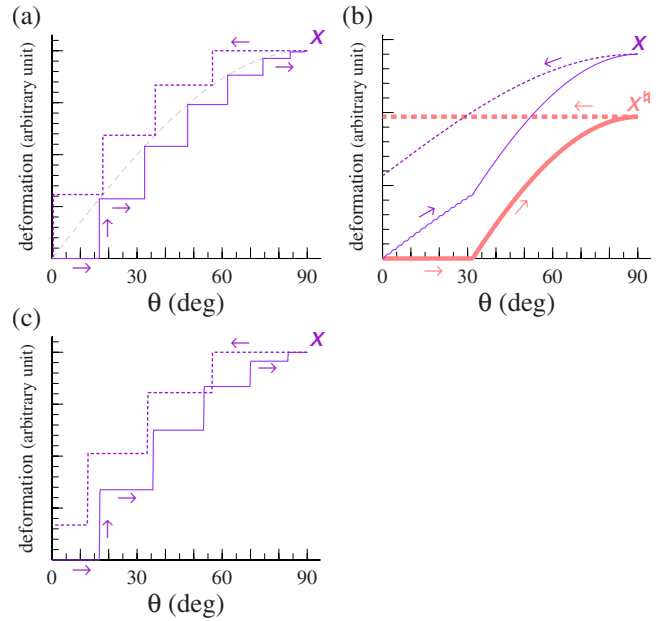


FIG. 7. (Color online) Mechanical hysteresis in Duran's brick. The deformation $x$ is plotted against the inclination $\theta$, with a solid line for the forward process (increasing $\theta$) and with a broken line for the backward process. (a) Duran's solution [23] in the case of static Coulomb friction. (b) Bingham-like case with Eqs. (55a) and (55b). In addition to $x$, the natural length of the Bingham-like element, $x^\natural$, is delineated in thick (red) lines. (c) A solution of Eq. (56) exhibiting Coulomb-like stick-slip motion.

a function of the inclination angle $\theta$, when $\theta$ varies slowly in time.

Suppose that the wall starts from the horizontal position ($\theta = 0$) and that we know the initial value of $x$, which we denote by $x_0$. For a while $x$ is stuck to $x_0$, until the "yield" criterion

$$|mG \sin \theta - kx| = \mu_s mG \cos \theta$$

is attained and the brick starts to slip. We assume the viscous resistance $-c\dot{x}$ and neglect the dynamic Coulomb friction for simplicity [50], so that the brick moves according to

$$m\frac{d^2 x}{dt^2} = -c\frac{dx}{dt} - kx + mG \sin \theta \quad (\text{brick in motion})$$

and eventually stops. This process is repeated while $\theta$ increases, as is shown in Fig. 7(a) with a solid line (each slip is assumed to stop when $kx = mG \sin \theta$ according to Duran [23]). If $\theta$ starts from $\pi/2$ and decreases slowly in time, a similar but different stick-slip motion occurs, as depicted by the broken line. Thus the system exhibits mechanical hysteresis due to static friction.

Now let us compare this mechanical hysteresis with the behavior of the system in Fig. 6(b), where the Coulomb friction is replaced by a discrete-element analog of Bingham-like elastoplasticity. Its behavior is defined by combining Eqs. (14) and (15a) or (15b) with

$$\tau^{-1} = \nu(T) \sim \begin{cases} 0 & [E(T) < \text{threshold}] \\ \tau_0^{-1} & [E(T) \geqslant \text{threshold}], \end{cases} \quad (54)$$

which is a discrete-element version of Eq. (1), with $E(T) = T^2/(2\kappa)$ standing for the elastic energy stored in this element. The governing equation of this system is summarized as

$$\frac{dx^{\natural}}{dt} = \nu(T)(x - x^{\natural}), \quad (55a)$$

$$m\frac{d^2x}{dt^2} = -T - kx + mG \sin \theta, \quad (55b)$$

supplemented with $T = \kappa(x - x^{\natural})$. As for $\nu(T)$, a Lipschitz-continuous form analogous to Eq. (29) is assumed. By numerical integration of Eqs. (55a) and (55b) with $\theta$ increased slowly from zero to $\pi/2$ and then decreased back, we obtain the result shown in Fig. 7(b). The thick solid line indicates that a shift of $x^{\natural}$ has occurred during the process of increasing $\theta$, and this shift was not recovered at all when $\theta$ was decreased (thick broken line). In addition, when $\theta$ has returned to zero, there remains a difference in $x$ and $x^{\natural}$, indicating residual pressure in this case. Thus, again, a hysteresis due to static indeterminacy is observed. There is an important difference, however, that the curves in Fig. 7(b) are much less singular than those in Fig. 7(a). In other words, at least for the values of the parameters and the functional form of $\nu(T)$ used in this calculation, no stick-slip behavior is observed. This is probably related to the property of the Bingham model, which predicts continuous shear stress across the yield front in quite general cases [26].

It is an interesting attempt to reformulate the stick-slip motion subject to static Coulomb friction in terms of $\nu$, to obtain a (formally) unified equation:

$$\frac{dv}{dt} = \nu(v, F, N)\left(\frac{F}{c} - v\right), \quad (56)$$

with

$$v = \frac{dx}{dt}, \quad F = -kx + mG \sin \theta, \quad N = mG \cos \theta.$$

A naive choice for $\nu$ is

$$\nu(v, F, N) = \begin{cases} 0 & (v = 0 \text{ and } |F| < \mu_s N) \\ \tau_0^{-1} = c/m & (\text{otherwise}). \end{cases}$$

Though this function is too singular to constitute a mathematically sound evolutional equation, adoption of continuous interpolation similar to Eq. (29) enables the numerical integration of Eq. (56), resulting in stick-slip motion shown in Fig. 7(c). Note that, in Eq. (56), the relaxation is attributed to the momentum, but this seems to be somewhat unnatural if we consider that friction is a property of the interface while momentum concerns the whole mass of the body. Rather, in analogy to Eq. (55a) where relaxation is attributed to $x^{\natural}$, it seems more appropriate to introduce a variable describing the state of the interface (possibly similar to the one introduced by Carlson and Batista [27]) and prescribe its

relaxation. This is beyond the scope of the present work, however.

In soil mechanics, a continuum version of Coulomb friction is known as Mohr-Coulomb plasticity [28]. Its application to the statics of granular materials is usually supplemented with the limit-state assumption, which states that the ratio of the shear stress to the normal stress is just below the threshold value everywhere. This assumption makes it possible to evaluate the stress field without introducing granular elasticity that is not understood very well. However, this theory encounters a number of difficulties, as is discussed by Kamrim and Bazant [29]. According to this theory, the static stress field is subject to a nonlinear hyperbolic system of equations [not in space-time but in the $(x, y)$ plane] which predicts a highly discontinuous stress field. The solution for the velocity field can be even more singular, which seems abnormal both physically and mathematically. Sometimes it also fails to satisfy the boundary conditions. Kamrim and Bazant [29] have shown that these difficulties can be avoided, within the framework of Mohr-Coulomb plasticity with the limit-state assumption, by introducing diffusive motions via mesoscale objects called "spots." In spite of this successful result, the theory is not free from the limitation due to the limit-state assumption, as the authors themselves admit that clearly it breaks down in some cases.

Kamrim and Bazant [29] state repeatedly that the introduction of elasticity will solve the difficulties of the Mohr-Coulomb plastic model. To some extent, this remark applies to Bingham plasticity as well. For example, the original Bingham model exhibits a singular behavior due to the lack of elasticity, in the sense that the propagation speed of yield front is infinitely large [30]. Treatment of residual stress would be also very difficult, if not impossible, without considering finite elasticity. This is why we sought to develop an elastoplastic paste model from the beginning.

The present theory is conceptually akin to the models of the memory effect in polymeric materials [10,31]. Miyamoto *et al.* [10] studied the memory effect in the glass transition of vulcanized rubber. They explained their experimental results with a Maxwell-like model,

$$\sigma(t) = \sigma_{\text{rubber}}(\mathcal{T}(t), \gamma(t)) + S_{\text{glass}}\int_{-\infty}^{t} [\gamma(t) - \gamma(t')]\frac{\partial \mathcal{G}(\tilde{t})}{\partial t'}dt', \quad (57)$$

where $\sigma$ is stress, $\mathcal{T}$ is temperature, $\gamma$ is strain, $\mathcal{G}(\cdot)$ is normalized relaxation function, and $\tilde{t}$, defined by

$$\tilde{t} = \tilde{t}(t, t') = \int_{t'}^{t} \frac{du}{\tau(\mathcal{T}(u), \gamma(u))},$$

stands for the intrinsic time lapse. The effect of temperature control (quenching and reheating) is expressed via $\tau$, which changes the pace of the intrinsic time $t'$ and thereby affects the memory function in Eq. (57). Note that $\gamma(t')$ in the integral can be read as the natural length of a spring born at the time $t'$. In this sense, Eq. (14) can be regarded as a simplified version of Eq. (57), though there is an important difference that the memory in Eq. (14) is ascribed to a single variable

$x^{\natural}$, while Eq. (57) can memorize more about the history of $\gamma(t')$. The "memory capacity" of Eq. (57) depends on the property of the relaxation function $\mathcal{G}(\cdot)$. Using a sum of two exponential functions, which implies double relaxation, Miyamoto *et al.* [10] has successfully reproduced the memory effect, including the effect of aging. In the present model, contrastively, the relaxation time $\tau$ is assumed to be a single scalar function. Instead, the spatial distribution of $\alpha$ and the effects of nonlinear elasticity are taken into account, thus enabling the creation and storage of the streamwise tension.

The idea of ascribing the memory to the plastic shift in the neutral point of elasticity, corresponding to $\alpha$ in Eqs. (38) and (44a), $x^{\natural}$ in Eqs. (14) and (55a), and $\gamma(t')$ in Eq. (57), is also shared by Ohzono *et al.* [31]. They studied microwrinkle patterns produced on a platinum-coated elastomer surface, governed by the competition between the restoring force of the platinum tending to be less curved and that of the elastomer that aims to shrink back. At room temperature, application of a uniaxial compression force breaks the force balance and changes the wrinkle pattern, but the original pattern is retrieved after the external force is removed. Contrastively, a protocol involving higher temperature (annealing-cooling-unloading protocol) changes the wrinkle pattern, introducing strong anisotropy. The new pattern is less stable to external forcing at room temperature, suggesting the presence of multiple metastable states. These experimental results are compared with a model prescribing the minimization of the elastic energy as a functional of the surface elevation $z=z(x,y)$,

$$U[z] = U_{\text{bending}} + U_{\text{in-plane}} + U_{\text{substrate}},$$

$$U_{\text{substrate}} = \int \{a(z-z_m)^2 + b(z-z_m)^4\}dxdy, \qquad (58)$$

where $U_{\text{bending}}$ and $U_{\text{in-plane}}$ are the potentials of bending and in-plane deformation of the platinum layer, $U_{\text{substrate}}$ is the potential of the substrate (with the constants $a$ and $b$ specified explicitly in terms of the material constants of the elastomer), and $z_m=z_m(x,y)$ represents the neutral point of $U_{\text{substrate}}$. Correspondence with Eq. (14) is obvious. The memory is carried by spatial distribution of $z_m$, which is fixed at the room temperature but is subject to plastic flow in the annealing-cooling-unloading protocol.

Generally, in elastic systems with more than several degrees of freedom (and particularly in continua), a shift in the neutral point introduces mechanical frustration. In the case of Ohzono *et al.* [31], it modifies the existing frustration, introducing multiple stability. In addition, spatial heterogeneity of $\alpha$ and $\beta$ in Eq. (37) is equivalent to the continuous distribution of edge dislocations and screw dislocations, respectively [13,32,33]. Thus frustration is observed universally in systems admitting plasticity (in any sense of the word), ranging from granular matters to metal crystals and spin glasses. From this viewpoint, we understand Eq. (44a) as describing the dynamic creation and static retention of mechanical frustration, presenting a macroscopic analog of dislocation dynamics.

### C. Future directions

The present study is entirely based on macroscopic phenomenology. It predicts the *presence* of a macroscopic mechanism that leads to the type-I Nakahara effect, but it does not assert the *absence* of other mechanisms, such as the creation of bond fabric or microscopic texture. A possible scenario is that the microscopic bond structure is well represented by the macroscopic (hydrodynamic) variables, such as $\alpha$ and $\tilde{\sigma}$, so that the most important feature of the mechanism is already captured by the hydrodynamic equations. In other words, we expect something analogous to ferromagnetism, where the macroscopic magnetization represents the order parameter. We cannot deny the possibility that some pastes have "antiferromagnetic" bond structure, which makes the macroscopic description more difficult. Even in the "ferromagnetic" case, consideration of microscopic details may introduce some modification. For example, we have regarded the yield stress as a given constant, but this may possibly need to be modified, in the way similar to work hardening and the Bauschinger effect in metals [34]. The constitutive relations assumed in this paper require justification more certain than a physicist's intuition, either by microscopic analysis or thermodynamical inspection. It is worthwhile to consider an extension of microscopic theories for glassy liquids, such as the mode-coupling theory [35,36] and the pair distribution function theory [37], in the direction corresponding to that of direct-interaction approximation in fluid turbulence based on Lagrangian description [38–41], in search of microscopic expression for $g_{\natural}^{ij}$. Such a microscopic approach would also allow us to construct a model for pastes whose properties are not isotropic. It is expected, for example, that a model including competitive interaction between the natural metric and director field may clarify the type-II Nakahara effect.

Within the framework of the present model, an explanation of Eq. (53) that gives the magnitude of the residual $\alpha$ is an open question. It is also necessary to extend the present work in several respects. On one hand, the limitation to uniform flows must be removed. The stopping process is simulated in this paper by switching gravity off, but in real experiments the paste flow stops when the paste supply is cut. Simulation of this process requires the introduction of a variable layer thickness $h=h(x,t)$, where the flow and the stress fields depend on $x$ as well. This extension will clarify the relevance of different mechanisms, such as the one proposed by Otsuki [42] where the $x$ dependence of the plastic deformation is essential. The present model can be readily extended in this direction, though its numerical analysis will be much more difficult. Derivation of reduced equations, such as depth-averaging (corresponding to Shkadov model [43–45] in the film flows and Saint-Venant model [46,47] in civil engineering), will be worth considering.

On the side of experiments, it is desirable to realize a uniform slope flow by eliminating the boundary effect in the $y$ direction. It is also necessary to measure the paste properties, such as $S$ and $\sigma_{\text{Y}}$, so that a qualitative comparison between the theory and the experiment becomes possible. Finally, since the mechanism proposed in this paper is closely related to the nonlinear viscoelasticity, it will be highly sup-

portive to detect any indication of nonlinear viscoelasticity in the paste, such as Weissenberg effect.

### APPENDIX A: NOTES ON THE FORMULATION OF LAGRANGIAN CONTINUUM MECHANICS IN TERMS OF DIFFERENTIAL GEOMETRY

Here we summarize the minimal mathematical knowledge required to understand, for example, how to calculate each side of Eq. (11). Instead of going along the rather expensive highway of Riemannian differential geometry, we take a shortcut, making full use of the $n_d$-dimensional Euclidean space where the whole system is embedded.

#### 1. Contravariant vector components

For each instant (with $t$ fixed arbitrarily), the mapping from $\boldsymbol{\xi}$ to $\mathbf{r}$ provides an instantaneous curvilinear coordinate system. This is sometimes referred to as a *convected coordinate system* [48]. It is this coordinated system, and not the space, that is curved.

Provided that the mapping (5), for fixed $t$, is sufficiently smooth and locally invertible, we find that

$$\left\{ \frac{\partial \mathbf{r}}{\partial \xi}, \frac{\partial \mathbf{r}}{\partial \eta}, \frac{\partial \mathbf{r}}{\partial \zeta} \right\} \quad (\text{for } n_d = 3)$$

forms a set of local bases in the $n_d$-dimensional Euclidean space ($\mathbf{r}$ space). Then, an arbitrary vector field, say $\mathbf{f}$, can be expressed as

$$\mathbf{f} = \left[ \frac{\partial \mathbf{r}}{\partial \xi} \quad \frac{\partial \mathbf{r}}{\partial \eta} \quad \frac{\partial \mathbf{r}}{\partial \zeta} \right] \begin{bmatrix} f^\xi \\ f^\eta \\ f^\zeta \end{bmatrix} = f^\xi \frac{\partial \mathbf{r}}{\partial \xi} + f^\eta \frac{\partial \mathbf{r}}{\partial \eta} + f^\zeta \frac{\partial \mathbf{r}}{\partial \zeta}$$

or, in abbreviation with Einstein's contraction rule,

$$\mathbf{f} = f^i \partial_i \mathbf{r}. \tag{A1}$$

The coefficients ($f^i$) in Eq. (A1) are referred to as *contravariant components* of the vector field $\mathbf{f}$. According to the convention of differential geometry, the contravariant components are superscripted.

If the labeling variable is changed from $\boldsymbol{\xi}$ to $\bar{\boldsymbol{\xi}}$ (in terms of a continuous, one-to-one mapping independent of $t$), the bases are changed to

$$\frac{\partial \mathbf{r}}{\partial \bar{\xi}^i} = \frac{\partial \xi^j}{\partial \bar{\xi}^i} \frac{\partial \mathbf{r}}{\partial \xi^j}.$$

Meanwhile the change from ($f^i$) to ($\bar{f}^i$) occurs in such a way that it cancels the change in the bases (therefore the name "contravariant"), so that the vector $\mathbf{f}$ itself remains unaffected:

$$\mathbf{f} = f^i \frac{\partial \mathbf{r}}{\partial \xi^i} = \bar{f}^i \frac{\partial \mathbf{r}}{\partial \bar{\xi}^i}.$$

An equation describing the relations between physical quantities should be independent of the choice of labeling variables. This is assured if and only if every term on both sides of the equation has the same behavior in regard to the relabeling. For example,

$$a^i = 2b^i$$

is acceptable, while

$$a^i \overset{?}{=} b^i + 2$$

is not (we cannot add a scalar 2 to a contravariant vector component $b^i$).

A second-order tensor, say $\mathbf{P}$, can be expressed as

$$\mathbf{P} = P^{ij}(\partial_i \mathbf{r}) \otimes (\partial_j \mathbf{r}), \tag{A2}$$

where $\otimes$ is the tensor product, such that

$$\mathbf{a} \cdot (\mathbf{b} \otimes \mathbf{c}) = (\mathbf{c} \otimes \mathbf{b}) \cdot \mathbf{a} = (\mathbf{a} \cdot \mathbf{b})\mathbf{c}.$$

The contravariant components ($P^{ij}$) are subject to the same kind of change as the product of two contravariant vector components, so that $\mathbf{P}$ remains unaffected by the relabeling. Note that Kronecker's delta with superscripts, $\delta^{ij}$, does not behave properly in regard to relabeling and therefore is not acceptable as a physically meaningful tensor.

#### 2. Dual basis and covariant vector components

As has been stated, we assume that the mapping from $\boldsymbol{\xi}$ to $\mathbf{r}$ is smooth and invertible. Therefore it makes sense to define

$$\nabla \xi^i = \frac{\partial \xi^i}{\partial \mathbf{r}}; \tag{A3}$$

a nabla without subscript, $\nabla$, is a mere abbreviation for $\partial/\partial \mathbf{r}$, i.e., the gradient operator in the $\mathbf{r}$ space. Evidently $\{\nabla \xi^i\}$ is the dual basis of $\{\partial_i \mathbf{r}\}$:

$$(\partial_i \mathbf{r}) \cdot \nabla \xi^j = \delta_i^j \tag{A4}$$

due to the chain rule. Also

$$(\nabla \xi^i) \otimes \partial_i \mathbf{r} = \mathbb{1}, \tag{A5}$$

where $\mathbb{1}$ denotes the unit tensor in the $\mathbf{r}$ space. Note that Eq. (A5) holds thanks to the fact that the embedding $\mathbf{r}$ space has the same dimension as the $\boldsymbol{\xi}$ space [otherwise $(\nabla \xi^i) \otimes \partial_i \mathbf{r}$ would be a projection operator whose rank is lower than the dimension of the $\mathbf{r}$ space]. The dual basis allows us to find the contravariant components of a given vector field, say $\mathbf{f}$, by

$$f^i = \mathbf{f} \cdot \nabla \xi^i; \tag{A6}$$

substitution of this expression into the right-hand side of Eq. (A1) recovers $\mathbf{f}$ due to Eq. (A5).

As opposed to the contravariant components ($f^i$) of a vector field $\mathbf{f}$, we define its covariant components ($f_i$) by

$$\mathbf{f} = f_i \nabla \xi^i. \tag{A7}$$

It is easily confirmed that

$$f_i = (\partial_i \mathbf{r}) \cdot \mathbf{f} = g_{ij} f^j,$$

where $g_{ij}$ stands for the Euclidean metric tensor defined in Eq. (8).

Using Eqs. (8) and (A5), we identify ($g_{ij}$) with covariant components of the Euclidean unit tensor,

$$g_{ij}(\nabla \xi^i) \otimes (\nabla \xi^j) = \mathbb{1}.$$

The contravariant components of $\mathbb{1}$ comprise the inverse matrix of ($g_{ij}$), denoted by ($g^{ij}$), which leads to Eq. (24). This implies that ($\tilde{p} g^{ij}$) in Eq. (16) and ($K g^{ij}$) in Eq. (19) stand for isotropic tensors.

### 3. Covariant derivative

The momentum equation (11), represented in terms of contravariant components, contains $\nabla_j$ which generally differs from $\partial_j = \partial / \partial \xi^j$. This "nabla with a subscript" is referred to as the *covariant derivative*. When the space is curved, it is not a trivial problem to define the covariant derivative in an appropriate way. Fortunately, since the space itself is now flat, we can now define $\nabla_j$ as a component of a simple "gradient" using $\nabla = \partial / \partial \mathbf{r}$. For a scalar field, say $\varphi$, its gradient is

$$\nabla \varphi = \frac{\partial \varphi}{\partial \mathbf{r}} = \frac{\partial \xi^i}{\partial \mathbf{r}} \frac{\partial \varphi}{\partial \xi^i} = (\nabla \xi^i) \partial_i \varphi;$$

the covariant derivative of $\varphi$ is given by the covariant components (i.e., the coefficients for $\nabla \xi^i$) of $\nabla \varphi$,

$$\nabla_i \varphi = \partial_i \varphi. \tag{A8}$$

The covariant derivative of a vector field is slightly more complicated. For $\mathbf{f}$ given in terms of its contravariant components ($f^i$), the gradient is

$$\text{grad } \mathbf{f} = \nabla \otimes \mathbf{f} = [(\nabla \xi^j) \partial_j] \otimes (f^i \partial_i \mathbf{r}) = (\nabla \xi^j) \otimes \partial_j (f^i \partial_i \mathbf{r});$$

we define the covariant derivative $\nabla_j f^i$ by

$$\partial_j (f^i \partial_i \mathbf{r}) = (\nabla_j f^i) \partial_i \mathbf{r} \tag{A9}$$

so that

$$\text{grad } \mathbf{f} = (\nabla_j f^i)[(\nabla \xi^j) \otimes \partial_i \mathbf{r}].$$

A handy way to evaluate $\nabla_j f^i$, in the present case, is to calculate the Cartesian components of $\mathbf{f} = f^i \partial_i \mathbf{r}$ and then to differentiate them with $\xi^j$, which yields the left-hand side of Eq. (A9). For those who disdain to depend on the embedding $\mathbf{r}$ space, there is a more orthodox way based on a formula

$$\nabla_i f^j = \partial_i f^j + \Gamma^j_{ik} f^k,$$

with $\Gamma^j_{ik}$ referred to as the *Levi-Cività connection* (also

known as the *Christoffel symbol* when it is calculated from $\partial_i \partial_j \mathbf{r}$). Both ways lead to the same result.

The momentum equation (11) contains a term arising from the divergence of stress tensor,

$$\text{div } \mathbf{P} = \lim \frac{1}{\Delta V} \int_{\partial(\Delta V)} \mathbf{P} \cdot \mathbf{n} dS = \nabla \cdot {}^t \mathbf{P},$$

where ${}^t(\cdot)$ denotes transposition (practically it could be omitted, as $\mathbf{P}$ is symmetric). Substitution of $\mathbf{P} = P^{ij}(\partial_i \mathbf{r}) \otimes (\partial_j \mathbf{r})$ and $\nabla = (\nabla \xi^k) \partial_k$ yields

$$\begin{aligned}
\text{div } \mathbf{P} &= \frac{\partial}{\partial \mathbf{r}} \cdot {}^t[P^{ij}(\partial_i \mathbf{r}) \otimes (\partial_j \mathbf{r})] \\
&= (\nabla \xi^k) \cdot {}^t\{\partial_k [P^{ij}(\partial_i \mathbf{r}) \otimes (\partial_j \mathbf{r})]\} \\
&= \{\partial_k [P^{ij}(\partial_i \mathbf{r}) \otimes (\partial_j \mathbf{r})]\} \cdot \nabla \xi^k, \tag{A10}
\end{aligned}$$

where the last equal sign follows from the definition of the transposition. At this stage, we need the covariant derivative for ($P^{ij}$). Taking into account a general postulation that any formula for a second-order tensor should apply to the tensor product of two vectors as well, we find the appropriate definition to be

$$\partial_k [P^{ij}(\partial_i \mathbf{r}) \otimes (\partial_j \mathbf{r})] = (\nabla_k P^{ij})(\partial_i \mathbf{r}) \otimes (\partial_j \mathbf{r}) \tag{A11}$$

so that

$$\begin{aligned}
\text{div } \mathbf{P} &= (\nabla_k P^{ij})[(\partial_i \mathbf{r}) \otimes (\partial_j \mathbf{r})] \cdot (\nabla \xi^k) \\
&= (\nabla_k P^{ij})(\partial_i \mathbf{r}) \delta^k_j = (\nabla_j P^{ij}) \partial_i \mathbf{r}.
\end{aligned}$$

Again, $\nabla_k P^{ij}$ can be evaluated either in terms of the Cartesian components of $\mathbf{P}$ or with a formula

$$\nabla_k P^{ij} = \partial_k P^{ij} + \Gamma^i_{kl} P^{lj} + \Gamma^j_{kl} P^{il}.$$

### 4. Velocity and acceleration

Up to the present point in this appendix, we have treated the spatial aspect of the mapping from $(\boldsymbol{\xi}, t)$ to $\mathbf{r}$ with $t$ fixed. Now we will detail the temporal aspect of this mapping. Let us recall that $\partial_t$ stands for the Lagrange derivative,

$$\partial_t(\cdot) = \left( \frac{\partial \cdot}{\partial t} \right)_{\boldsymbol{\xi}},$$

unless specified otherwise [in Eq. (4), for example]. The velocity $\mathbf{v}$ is then given by Eq. (6), and the (material) acceleration is

$$\partial_t^2 \mathbf{r} = \partial_t \mathbf{v} = \partial_t(v^i \partial_i \mathbf{r}) \tag{A12}$$

as is seen on the left-hand side of the momentum equation just above Eq. (11). Taking the time dependence of $\partial_i \mathbf{r}$ into account, we evaluate the acceleration as

$$\begin{aligned}
\partial_t(v^i \partial_i \mathbf{r}) &= (\partial_t v^i) \partial_i \mathbf{r} + v^i \partial_t \partial_i \mathbf{r} \\
&= (\partial_t v^i) \partial_i \mathbf{r} + v^i \partial_i \partial_t \mathbf{r} = (\partial_t v^i) \partial_i \mathbf{r} + v^i \partial_i \mathbf{v}
\end{aligned}$$

and rewrite the last term, which contains $\partial_i \mathbf{v}$, with the covariant derivative. Thus we find

$$\partial_t \mathbf{v} = (\partial_t v^i + v^j \nabla_j v^i) \partial_i \mathbf{r}. \qquad (A13)$$

The contravariant component of Eq. (A13), multiplied by $\rho$, gives the left-hand side of Eq. (11).

### 5. Derivation of Eq. (40)

Next, we study a concrete example to see how the momentum equation (11) is evaluated. With the mapping $\boldsymbol{\xi} \mapsto \mathbf{r}$ specified as Eq. (34), the momentum equation (11) is to be reduced to Eq. (40).

Equation (34) readily yields the velocity in Eq. (35) and the local basis

$$\partial_\xi \mathbf{r} = \begin{bmatrix} 1 \\ 0 \end{bmatrix}_{\mathrm{C}}, \quad \partial_\zeta \mathbf{r} = \begin{bmatrix} X' \\ 1 \end{bmatrix}_{\mathrm{C}}, \qquad (A14)$$

where $U$ and $X'$ are understood as

$$U = \partial_t X(\zeta, t), \quad X' = \partial_\zeta X(\zeta, t).$$

Substituting Eq. (A14) into Eq. (8) yields ($g_{ij}$) in Eq. (36).

The natural metric tensor is parametrized as Eq. (37); this expression becomes identical to that for **g** if $\alpha = 0$ and $\beta = X'$. The components of the inverse natural metric tensor are then

$$\mathbf{g}_\natural = \begin{bmatrix} g_\natural^{\xi\xi} & g_\natural^{\xi\zeta} \\ g_\natural^{\zeta\xi} & g_\natural^{\zeta\zeta} \end{bmatrix} = \begin{bmatrix} (1+\beta^2)e^\alpha & -\beta \\ -\beta & e^{-\alpha} \end{bmatrix}. \qquad (A15)$$

By using Eqs. (A14) and (A15), the term $g_\natural^{ij}(\partial_i \mathbf{r}) \otimes (\partial_j \mathbf{r})$ in Eq. (25) is calculated to be

$$\begin{aligned}
g_\natural^{ij}(\partial_i \mathbf{r}) \otimes (\partial_j \mathbf{r}) &= (1+\beta^2)e^\alpha(\partial_\xi \mathbf{r}) \otimes (\partial_\xi \mathbf{r}) - \beta[(\partial_\xi \mathbf{r}) \otimes (\partial_\zeta \mathbf{r}) \\
&\quad + (\partial_\zeta \mathbf{r}) \otimes (\partial_\xi \mathbf{r})] + e^{-\alpha}(\partial_\zeta \mathbf{r}) \otimes (\partial_\zeta \mathbf{r}) \\
&= (1+\beta^2)e^\alpha \begin{bmatrix} 1 & 0 \\ 0 & 0 \end{bmatrix}_{\mathrm{C}} - \beta \begin{bmatrix} 2X' & 1 \\ 1 & 0 \end{bmatrix}_{\mathrm{C}} \\
&\quad + e^{-\alpha} \begin{bmatrix} X'^2 & X' \\ X' & 1 \end{bmatrix}_{\mathrm{C}} \\
&= \begin{bmatrix} (1+\beta^2)e^\alpha - 2\beta X' + e^{-\alpha}X'^2 & e^{-\alpha}X' - \beta \\ e^{-\alpha}X' - \beta & e^{-\alpha} \end{bmatrix}_{\mathrm{C}}.
\end{aligned}$$
$$(A16)$$

Taking notice of the $(x,z)$ component of this expression, which corresponds to $\sigma_{xz}/S$, we introduce $\tilde{\sigma}$ given by Eq. (39). Then Eq. (25) yields a concrete expression for $\overleftrightarrow{\sigma}$ shown in Eq. (38).

In the present setup, the nabla operator is given by

$$\nabla = \frac{\partial}{\partial \mathbf{r}} = \frac{\partial \xi}{\partial \mathbf{r}} \partial_\xi + \frac{\partial \zeta}{\partial \mathbf{r}} \partial_\zeta, \qquad (A17)$$

where

$$\frac{\partial \xi}{\partial \mathbf{r}} = \begin{bmatrix} 1 \\ -X' \end{bmatrix}_{\mathrm{C}}, \quad \frac{\partial \zeta}{\partial \mathbf{r}} = \begin{bmatrix} 0 \\ 1 \end{bmatrix}_{\mathrm{C}}.$$

Then the divergence in the momentum equation (11) is evaluated in terms of the Cartesian components in the **r** space:

$$\begin{aligned}
-\operatorname{div} \mathbf{P} &= -\begin{bmatrix} 1 \\ -X' \end{bmatrix}_{\mathrm{C}} \partial_\xi \tilde{p} - \begin{bmatrix} 0 \\ 1 \end{bmatrix}_{\mathrm{C}} \partial_\zeta \tilde{p} \\
&\quad + S\left( \partial_\zeta \begin{bmatrix} e^\alpha(1+\tilde{\sigma}^2)-1 & \tilde{\sigma} \\ \tilde{\sigma} & e^{-\alpha}-1 \end{bmatrix}_{\mathrm{C}} \right) \begin{bmatrix} 0 \\ 1 \end{bmatrix}_{\mathrm{C}} \\
&= -\left( \begin{bmatrix} 1 & 0 \\ -X' & 1 \end{bmatrix} \begin{bmatrix} \partial_\xi \tilde{p} \\ \partial_\zeta \tilde{p} \end{bmatrix} \right)_{\mathrm{C}} + S \begin{bmatrix} \partial_\zeta \tilde{\sigma} \\ -e^{-\alpha}\partial_\zeta \alpha \end{bmatrix}_{\mathrm{C}},
\end{aligned}$$

where it is taken into account that $\alpha$, $\beta$, and $X'$ are independent of $\xi$. As for the left-hand side of the momentum equation, it is easily shown that

$$\partial_t \mathbf{v} = \begin{bmatrix} \partial_t U \\ 0 \end{bmatrix}_{\mathrm{C}}.$$

Calculating the inner product of the momentum equation with $\partial_\xi \mathbf{r}$, we obtain

$$\rho \partial_t U = -\partial_\xi \tilde{p} + S \partial_\zeta \tilde{\sigma} + \rho G \sin \theta; \qquad (A18)$$

similarly, the inner product with $\partial_\zeta \mathbf{r}$ yields

$$\rho X' \partial_t U = -\partial_\zeta \tilde{p} + S(X' \partial_\zeta \tilde{\sigma} - e^{-\alpha}\partial_\zeta \alpha) + \rho G(X' \sin \theta - \cos \theta). \qquad (A19)$$

From Eq. (A19), we find that $\partial_\zeta \tilde{p}$ is independent of $\xi$.

Here we use a concrete formulation of the free-surface boundary condition for **P** (neglecting surface tension and surface contamination),

$$P^{ij}n_j|_{\zeta=H} = p_{\mathrm{atm}}g^{ij}n_j, \qquad (A20)$$

where $p_{\mathrm{atm}}$ denotes the (constant) atmospheric pressure, which can be set equal to zero without loss of generality, and $n_j$ stands for the covariant component of the surface normal vector, which is given by $\mathbf{n} = \nabla(z-H)$ so that $n_j = \nabla_j z = \partial z/\partial \xi^j$ for the present case. For $\tilde{p}$, the boundary condition (A20) reads

$$(\tilde{p} - \sigma_{zz})|_{\zeta=H} = p_{\mathrm{atm}}(=0), \qquad (A21)$$

with $\sigma_{zz} = S(e^{-\alpha}-1)$ according to Eq. (38). Evidently, Eq. (A21) is also independent of $\xi$. Then $\tilde{p}$ turns out to be totally independent of $\xi$, which implies that $\partial_\xi \tilde{p}$ in Eq. (A18) vanishes, leading to Eq. (40).

### 6. Derivation of Eqs. (41) and (42)

The relaxation of $\mathbf{g}^\natural$ is described by Eq. (17) or, equivalently, Eq. (19). We substitute **g** parametrized as Eq. (36) and $\mathbf{g}^\natural$ as Eq. (37) into Eq. (19), together with

$$\tau \partial_t \begin{bmatrix} g_\natural^{\xi\xi} & g_\natural^{\xi\zeta} \\ g_\natural^{\zeta\xi} & g_\natural^{\zeta\zeta} \end{bmatrix} = \begin{bmatrix} (1+\beta^2)e^\alpha & 0 \\ 0 & -e^{-\alpha} \end{bmatrix} \tau \partial_t \alpha \\ + \begin{bmatrix} 2\beta e^\alpha & -1 \\ -1 & 0 \end{bmatrix} \tau \partial_t \beta.$$

Equating each component of the matrix yields *three* equations for two variables $\alpha$ and $\beta$; the equations are consistent (solvable) only when $K$ is set appropriately, which is calculated, according to Eq. (28), as

$$K = \frac{2}{2\cosh\alpha + e^{\alpha}\tilde{\sigma}^2} = \frac{2}{2+\varepsilon}, \qquad \text{(A22)}$$

with $\varepsilon$ given by Eq. (43) in the two-dimensional case. From the $\zeta\zeta$ component and the $\zeta\xi$ component of Eq. (19) we obtain Eq. (41) and Eq. (42), respectively.

## APPENDIX B: VARIATION OF THE ELASTIC ENERGY $E$

Equation (16) is obtained from elastic energy $E$ in Eq. (23) by calculating its variation in regard to $\mathbf{r} = \mathbf{r}(\boldsymbol{\xi})$ under the constraint $\det\mathbf{g} = 1$. In this calculation we use

$$\delta(\det\mathbf{g}) = (\det\mathbf{g})g^{ij}\delta g_{ij},$$

$$\delta g_{ij} = \delta(\partial_i\mathbf{r}\cdot\partial_j\mathbf{r}) = (\partial_i\delta\mathbf{r})\cdot\partial_j\mathbf{r} + \partial_i\mathbf{r}\cdot(\partial_j\delta\mathbf{r}),$$

and

$$\partial_j\sqrt{\det\mathbf{g}} = \frac{1}{2}\sqrt{\det\mathbf{g}}\,g^{kl}\partial_j g_{kl} = \sqrt{\det\mathbf{g}}(\nabla\xi^k)\cdot\partial_j\partial_k\mathbf{r}.$$

The result is as follows:

$$\delta\int E\,dV = \frac{1}{2}S\delta\int (g_{ij}g^{ij} - n_d)\sqrt{\det\mathbf{g}}\,d^{n_d}\boldsymbol{\xi} = \frac{1}{2}S\int \left(g^{ij}_\natural + \frac{1}{2}\varepsilon g^{ij}\right)\delta g_{ij}\sqrt{\det\mathbf{g}}\,d^{n_d}\boldsymbol{\xi} = S\int \left(g^{ij}_\natural + \frac{1}{2}\varepsilon g^{ij}\right)(\partial_i\mathbf{r})\cdot(\partial_j\delta\mathbf{r})\sqrt{\det\mathbf{g}}\,d^{n_d}\boldsymbol{\xi}$$

$$= -S\int \left\{\partial_j\left[\left(g^{ij}_\natural + \frac{1}{2}\varepsilon g^{ij}\right)\sqrt{\det\mathbf{g}}\,\partial_i\mathbf{r}\right]\right\}\cdot\delta\mathbf{r}\,d^{n_d}\boldsymbol{\xi} = -S\int \left\{(\nabla\xi^k)\cdot\partial_k\left[\left(g^{ij}_\natural + \frac{1}{2}\varepsilon g^{ij}\right)(\partial_i\mathbf{r})\otimes(\partial_j\mathbf{r})\right]\right\}\cdot\delta\mathbf{r}\sqrt{\det\mathbf{g}}\,d^{n_d}\boldsymbol{\xi}$$

$$\text{(B1)}$$

and

$$\delta\int p'(\sqrt{\det\mathbf{g}} - 1)dV = \delta\int p'(\sqrt{\det\mathbf{g}} - 1)\sqrt{\det\mathbf{g}}\,d^{n_d}\boldsymbol{\xi} = \int p'\left(1 - \frac{1}{2\sqrt{\det\mathbf{g}}}\right)\delta(\det\mathbf{g})d^{n_d}\boldsymbol{\xi}$$

$$= \int p'\left(\sqrt{\det\mathbf{g}} - \frac{1}{2}\right)2g^{ij}(\partial_i\mathbf{r})\cdot(\partial_j\delta\mathbf{r})\sqrt{\det\mathbf{g}}\,d^{n_d}\boldsymbol{\xi} = -\int \{\partial_j[p'(2\sqrt{\det\mathbf{g}} - 1)g^{ij}(\partial_i\mathbf{r})\sqrt{\det\mathbf{g}}]\}\cdot\delta\mathbf{r}\,d^{n_d}\boldsymbol{\xi}$$

$$= -\int \{(\nabla\xi^k)\cdot\partial_k[p'(2\sqrt{\det\mathbf{g}} - 1)g^{ij}(\partial_i\mathbf{r})\otimes(\partial_j\mathbf{r})]\}\cdot\delta\mathbf{r}\sqrt{\det\mathbf{g}}\,d^{n_d}\boldsymbol{\xi}, \qquad \text{(B2)}$$

which is summarized as

$$\delta\int [E - p'(\sqrt{\det\mathbf{g}} - 1)]dV = \int \{(\nabla\xi^k)\cdot\partial_k[P^{ij}(\partial_i\mathbf{r})\otimes(\partial_j\mathbf{r})]\}\cdot\delta\mathbf{r}\sqrt{\det\mathbf{g}}\,d^{n_d}\boldsymbol{\xi}, \qquad \text{(B3)}$$

with

$$P^{ij} = -S\left(g^{ij}_\natural + \frac{1}{2}\varepsilon g^{ij}\right) + p'(2\sqrt{\det\mathbf{g}} - 1)g^{ij} = -Sg^{ij}_\natural + (p' - E)g^{ij}, \qquad \text{(B4)}$$

where the last equal sign is due to $\sqrt{\det\mathbf{g}} = 1$. Then, rewriting the undetermined multiplier as $p' = \tilde{p} + E - S$, we obtain Eq. (16).

[1] M. C. Miguel and M. Rubi, *Jamming, Yielding, and Irreversible Deformation in Condensed Matter* (Springer-Verlag, Berlin, 2006).

[2] A. Nakahara and Y. Matsuo, Bussei Kenkyu **81**, 184 (2003) (in Japanese).

[3] A. Nakahara and Y. Matsuo, J. Phys. Soc. Jpn. **74**, 1362 (2005).

[4] A. Nakahara and Y. Matsuo, J. Stat. Mech.: Theory Exp. (2006), P07016.

[5] A. Nakahara and Y. Matsuo, Phys. Rev. E **74**, 045102(R) (2006).

[6] H. Kawazoe, K. Kanemura, and T. Ooshida (unpublished).

[7] L. D. Landau and E. M. Lifshitz, *Fluid Mechanics*, Theoretical Physics Vol. 6 (Butterworth-Heinemann, Oxford, 1987).

[8] H. Schlichting and K. Gersten, *Boundary Layer Theory*, 8th ed. (Springer-Verlag, Berlin, 2000).

[9] D. D. Joseph, *Fluid Dynamics of Viscoelastic Liquids* (Springer-Verlag, New York, 1990).

[10] Y. Miyamoto, K. Fukao, H. Yamao, and K. Sekimoto, Phys. Rev. Lett. **88**, 225504 (2002).

[11] K. Kruse, J. F. Joanny, F. Jülicher, J. Prost, and K. Sekimoto, Phys. Rev. Lett. **92**, 078101 (2004).

[12] K. Kruse, J. F. Joanny, F. Jülicher, J. Prost, and K. Sekimoto, Eur. Phys. J. E **16**, 5 (2005).

[13] T. Ooshida and K. Sekimoto, Phys. Rev. Lett. **95**, 108301 (2005).

[14] R. Hill, *The Mathematical Theory of Plasticity* (Oxford University Press, Oxford, 1950).

[15] H. Hencky, Z. Angew. Math. Mech. **4**, 323 (1924).

[16] A. Bennett, *Lagrangian Fluid Dynamics* (Cambridge University Press, Cambridge, England, 2006).

[17] J. E. Marsden and T. J. Hughes, *Mathematical Foundations of Elasticity* (Dover, New York, 1994) (published originally by Prentice-Hall, 1983).

[18] M. Nakahara, *Geometry, Topology, And Physics* (Institute of Physics, Bristol, 1990).

[19] E. H. Lee, J. Appl. Mech. **36**, 1 (1969).

[20] V. A. Lubarda and E. H. Lee, J. Appl. Mech. **48**, 35 (1981).

[21] E. C. Bingham, *Fluidity and Plasticity* (McGraw-Hill, New York, 1922).

[22] C. C. Mei and M. Yuhi, J. Fluid Mech. **431**, 135 (2001).

[23] J. Duran, *Sands, Powders, and Grains: An Introduction to the Physics of Granular Materials* (Springer-Verlag, New York, 2000), translated by Axel Reisinger.

[24] W. H. Press, B. P. Flannery, S. A. Teukolsky, and W. T. Vetterling, *Numerical Recipes in C* (Cambridge University Press, New York, 1988).

[25] I. S. Aranson and L. S. Tsimring, Rev. Mod. Phys. **78**, 641 (2006).

[26] K. Sekimoto, J. Non-Newtonian Fluid Mech.. **46**, 219 (1993).

[27] J. M. Carlson and A. A. Batista, Phys. Rev. E **53**, 4153 (1996).

[28] R. M. Nedderman, *Statics and Kinematics of Granular Materials* (Cambridge University Press, Cambridge, England, 1992).

[29] K. Kamrin and M. Z. Bazant, Phys. Rev. E **75**, 041301 (2007).

[30] K. Sekimoto, J. Non-Newtonian Fluid Mech. **39**, 107 (1991).

[31] T. Ohzono and M. Shimomura, Phys. Rev. E **72**, 025203(R) (2005).

[32] L. D. Landau and E. M. Lifshitz, *Theory of Elasticity*, Theoretical Physics Vol. 7 (Butterworth-Heinemann, Oxford, 1986).

[33] P. M. Chaikin and T. C. Lubensky, *Principles of Condensed Matter Physics* (Cambridge University Press, Cambridge, England, 1995).

[34] D. McLean, *Mechanical Properties of Metals* (Wiley, New York, 1962).

[35] K. Miyazaki and D. R. Reichman, Phys. Rev. E **66**, 050501(R) (2002).

[36] M. Fuchs and M. E. Cates, Phys. Rev. Lett. **89**, 248304 (2002).

[37] M. Otsuki and S. Sasa, J. Stat. Mech.: Theory Exp. ( 2006), L10004.

[38] U. Frisch, *Turbulence: The Legacy of A.N. Kolmogorov* (Cambridge University Press, Cambridge, England, 1995).

[39] R. H. Kraichnan, Phys. Fluids **8**, 575 (1965).

[40] Y. Kaneda, J. Fluid Mech. **107**, 131 (1981).

[41] S. Kida and S. Goto, J. Fluid Mech. **345**, 307 (1997).

[42] M. Otsuki, Phys. Rev. E **72**, 046115 (2005).

[43] V. Ya. Shkadov, Izv. Akad. Nauk SSSR, Mekh. Zhidk. Gaza **1**, 43 (1967).

[44] C. Ruyer-Quil and P. Manneville, Eur. Phys. J. B **6**, 277 (1998).

[45] H.-C. Chang and E. Demekhin, *Complex Wave Dynamics on Thin Films* (Elsevier, Amsterdam, 2002).

[46] A. J. C. de Saint-Venant, C. R. Acad. Sci. (Paris) **73**, 147 (1871).

[47] Y. Forterre and O. Pouliquen, J. Fluid Mech. **486**, 21 (2003).

[48] R. B. Bird, R. C. Armstrong, and O. Hassager, *Dynamics of Polymeric Liquids*, 2nd ed. (Wiley, New York, 1987), Vol. 1.

[49] According to Nakahara (private communication), a typical value of the Reynolds number in such cases is $R_H = 100$ on the basis of the layer thickness $H$, or $R_L = 2000$ on the basis of the horizontal length scale $L$ of the container. While $R_H = 100$ is typically not large enough to cause a transition to turbulence (in the usual sense of the word), we may expect a different kind of "turbulence" such as a two-dimensional chaotic flow maintained by horizontal forcing.

[50] The presence of the viscous drag is not explicitly stated in Duran's book [23], but it seems to be implicitly assumed by stating that $x$ stops at the position satisfying $kx = mG \sin \theta$.